MEASUREMENT OF SOIL MOISTURE AND COMPARISON TO EVAPOTRANSPIRATION ESTIMATION FOR UCSD ATHLETIC FIELDS

MICHAEL POGUE
SAM KELLER
JON SANGEL
YURI KROMSKY

Department of Mechanical and Aerospace Engineering, UC San Diego
April 27, 2009

Abstract

Evapotranspiration (ET) is water loss from a field by the combination of evaporation from the soil and transpiration through plants. It is the dominant source of water loss from fields. Accurate modeling of evapotranspiration enables better prediction of irrigation requirements. This study examines the soil moisture content of Warren Field by direct in-situ measurement using a soil probe. It directly calculates evapotranspiration from the field by average moisture content, and applies statistical and geostatistical analysis to evaluate and recommend optimum sample spacing. It further seeks to identify, qualitatively and quantitatively, correlation between soil temperature and soil moisture. Finally, it makes tentative irrigation recommendations.

The results show average evapotranspiration computed from in-situ measurements to be 2.8 mm of water per day, or 20mm per week. This is less than the 25 mm per week the field is currently irrigated, and seems to recommend a reduction. However these calculations are based on only three days data, with consistent, cool weather conditions. Unexpected irrigation interfered with data from a second week of measurements.

The variance of these measurements is independent of sample spacing, indicating that much wider spacing would yield similar results. The average volumetric water content and ground temperature of homogeneous athletic fields the size of the study area, 95m x 115m, can be reliably calculated from fewer than ten data points without introducing significant variance in comparison to calculations from 110 data points.

Soil moisture patterns seem to correlate significantly with ground temperature; however ground temperature measurements are not necessary for the accurate computation of ET. Neither is it necessary to resolve small features (on the order of 10m) in soil moisture variance to accurately compute total ET.

Attempts to calculate ET from environmental variables for comparison to in-situ measurements were inconclusive.

Contents

1. Introduction

1.1. Project Definition and Objectives

Water usage in arid climates, such as the American Southwest, is of critical importance as population density expands beyond the capacity of resources. Saving water has the twin benefits of lowering water bills, and reducing pressure on water supplies. Toward that end, it is important to schedule irrigation of UCSDs large athletic fields as seldom as possible while maintaining a healthy playing surface. This goal requires an accurate model of the rate of water loss from the field. The main route of water loss from large flat grassy fields is the combination of soil evaporation and plant transpiration, called evapotranspiration (ET). This study evaluates the rate of water loss by direct sampling of soil moisture over the days following irrigation, and by proven methods of estimation using meteorological data. It employs the methods established by the California Irrigation Management Information System (CIMIS), and by the Food and Agriculture Organization of the United Nations (FAO).

Everyone has seen sprinklers come on in the rain and wondered why. This study will lay the foundation to provide irrigation control based on actual soil water content.

2. Experimental Theory and Literature Survey

The main theoretical concepts in this study are the estimation of evapotranspiration, and the estimation of error sensitivity to sample spacing using geostatistics.

2.1. Evapotranspiration and Water Loss

Water lost from the soil of Warren field may escape by four routes: It may seep out the sides, it may seep down through the soil, it may evaporate from the soil or it may transpire through the plants. Of these, seepage through the sides is certainly a second-order effect given the size of Warren field and the slow motion of water in soil. Water lost through the bottom of the field to deep penetration will be neglected during this study. So for the model assumed here, water is lost from Warren field only through evaporation and transpiration, called together evapotranspiration (ET). The ratio of water lost to the two routes varies with conditions, but the overall water lost is accounted for in a single complex model. ET has units of volume. It is commonly expressed in units of length, which can be easily converted to irrigation needs.

2.1.1 Penman-Monteith Equation

Evapotranspiration was first modeled by Howard Penman in 1948. His equation, while valid in principle, has been modified to account for detail in the large number of variables. Several versions of the Penman equation exist, but the most widely used is the Penman-Monteith equation (Allen, 1997), whose inner workings are discussed here. The equation in its general form is

$$ET = \frac{\Delta(R_n - G) + \rho_a c_p \frac{e_s - e_a}{r_a}}{\lambda\left[\Delta + \gamma\left(1 + \frac{r_s}{r_a}\right)\right]} \quad (1)$$

In equation (1), R_n is the net radiation; G is the heat flux through the soil, which is much smaller than the radiation; ρ_a and c_p are the density and specific heat of air; e_s-e_a is the vapor pressure deficit, or the difference between the saturation vapor pressure of air at the current temperature and the actual vapor pressure—this is the measure of how much more moisture the air can handle; r_s and r_a are the surface and aerodynamic resistances; Δ is the slope of saturation pressure as a function of temperature; γ is the psychrometric constant, which relates the water partial pressure to air temperature; and λ is the heat of vaporization of water.

Equation (1) is an energy balance. The energy in from radiation, minus the energy lost to heat flux, plus the energy from the slope of the vapor gradient is divided by the energy required to vaporize water. The remaining terms are resistances (r_a, r_s) or unit conversion relationships (δ, γ).

2.1.2 Crop Factor and Stress Factor

The general form of the Penman-Monteith equation can be used for an arbitrary surface—the resistance terms

account for crop differences. In practice however, evapotranspiration is calculated for a reference surface, usually grass or alfalfa. The result is then multiplied by a crop-factor (K_c) to account for resistance differences. This system allows the splitting of micro climate data, which may be relatively constant over large areas, from crop-specific data, which fluctuates in space and time independent of weather. Thus calculations based on elaborate sensor systems are made more generally useful. Reference evapotranspiration is denoted ET_o. ET_o*K_c gives ET_c, which is the crop evapotranspiration assuming healthy plants and plentiful free water. The FAO recommends that for daily computations, K_c be divided into a soil coefficient and a basal plant coefficient.

$$K_c = K_e + K_b \tag{2}$$

These factors are readily available in tables, and modified using procedures provided by the FAO (Allen, 1997). They depend on the time of season.

When conditions are less than ideal, a stress factor, K_s, multiplies K_b to account for drops in plant water use due to drought, disease or other adverse conditions. The computation of the stress factor is, like the crop factor, straight forward but rather tedious. The final estimation of evapotranspiration based on ET_o is then

$$ET = ET_O \cdot K_s \cdot K_c \tag{3}$$

$$ET_{daily} = ETo(K_s \cdot K_b + K_e) \tag{4}$$

When the dual crop coefficient is computed, the stress factor applies only to the basal coefficient. For periods longer than a day, equation (3) is sufficient.

2.2. Soil Moisture Sampling

2.2.1 Background

This study in part quantifies the soil moisture content of a large field from a series of samples. Much work has been done on the difficulty of scaling data that may affect trends on areas of radically different magnitudes. Scale in geostatistical measurement is often in terms of support, spacing and extent. The size of the area under investigation is the extent—in this case, the extent is than 120m x 95m, or the two Westernmost Warren soccer fields. Support is the area or volume actually averaged in a sample. The support of the soil probes is point-like when compared to the extent of the soccer fields. Spacing, the distance between probes, is one of the goals of this study. It is often called lag, borrowing from the terminology of time-sampling.

While aircraft and satellite based sensing techniques provide averaged data over areas on the order of 10^2km or greater, they give little information about trends on scales below sensor resolution. Numerous studies make recommendations involving error versus sample spacing and frequency, however the test areas are heterogeneous and the studies assume little prior knowledge of soil moisture trends (Western and Blöschl, 1999, Famiglietti et al., 1997). Correlation lengths vary in heterogeneous zones, so spacing poses a complex problem. The Warren field comprises consistent turf, elevation, shade and soil type. The irrigation schedule of Warren is artificial with the obvious exception of rain. Consequently, given the slow speed of water movement through soil, correlation lengths may be as simple as irrigation zones. Still other studies (Rodriguez-Iturbe et al., 1995) examine the statistical patterns that arise from support scale, but make no spacing conclusions. The problem then is to recommend the optimal spacing of soil measurements in Warren field as a byproduct of this study. This recommendation is based on geostatistical analysis.

2.2.2 Geostatistics, Semi-Variogram[1]

Geostatistics concerns itself with quantifying error with respect the position of measurements. A geostatistical tool useful to evaluate optimal sensor spacing is the semi-variogram. In short, the semi-variogram is a plot of variance between measurements versus the distance between those measurements. Consider a square grid of moisture samples taken at 1m spacing. The quantity of interest is the volumetric moisture content as a function of x and y, $\mathbf{m}(x,y) \equiv \mathbf{m}(\mathbf{r})$. Throwing all measurements into one population for statistical analysis is incorrect unless we expect

[1] This section owes a large debt to Clark, 1979, chapters 1 and 2.

the moisture content to be constant across the field, which we do not. We look then for vector statistical measurement. The variance of measurements is defined, as in *scalar* statistics as

(5)

where μ is the mean. Since $\mathbf{m(r)}$ varies in space, this definition of the variance is useless. We look then at two samples, separated by a vector **h.** Under the assumptions that the measurements are close in time, and that the spacing is smaller than the scale of any trend, we take the difference of those two measurements, rather than the difference between the measurement and the mean.

(6)

An important feature of equation (6) is that *S* depends on not only distance but also direction. This reflects that the spatial derivatives $\delta\mathbf{m}/\delta x$ and $\delta\mathbf{m}/\delta y$ need not be equal, and the attending error need not be either. S is the mean variance of the set of sample pairs separated by the vector **h**. Figure 1 shows the pairs for the vector **h**=1m, and for **h**=2m in the x-direction. S is a scalar, and has the units of the sample measurement squared. S may be computed for many values of **h**, and plotted as a function of distance. Though semi-variograms depend on direction, if the quantity of interest is nearly isotropic, semi-variograms for different directions but equal length may be combined.

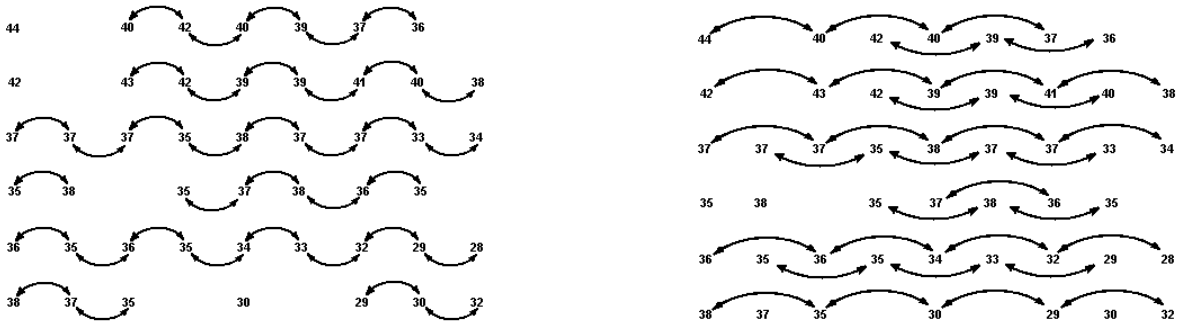

(a) (b)

Figure 1. Sampling grid showing point pairs included in the semi-variogram for the vector **h**=1m in the x-direction (a) and 2m in the x-direction (b). In geostatistics, the difference between sample values at each point pair is analogous to the difference between a sample and the mean in scalar statistics (Clark, 1979).

2.2.3 Sample Spacing

During data gathering, the spacing of the study samples was determined based on the time available. Two hours was the goal time to collect data. Approximately 2.5 hours were required to gather data for the two soccer fields at 20m lag. The analysis of semi-variograms, as well as computation of ET from partial data, i.e., removing samples from the population to simulate wider lag, shows how wide the lag can be for future studies while maintaining acceptable error.

3. Equipment and Setup

3.1. Overview

This study assumes water is lost only by evapotranspiration. Evapotranspiration is estimated by three methods.

- Approximate evapotranspiration calculation based on the modified Penman-Monteith energy balance equation using data from the California Irrigation Management Information System (CIMIS) weather station at Torrey Pines.
- Approximate evapotranspiration calculation based on the modified Penman-Monteith energy balance using data from the mobile tripod sensors.

- In-situ soil volumetric water content measurement using a moving station with a soil moisture probe.

Additionally, the tripod that holds the mobile station will be fitted with wheels, and a soil moisture probe for the mobile station selected.

3.2. Tripod

Students constructed a mobile tripod equipped with the sensor listed in Table 1[2].

Table 1. Sensor Mounting

Sensor	Tripod Mounting
Garmin 16-HVS Global Positioning System Receiver	Top, 2.3m high
Davis Standard and Industrial Anemometer	Side, 2.1 m high, .44m out
Dynamax ML2 Soil Moisture Probe	None
Campbell Scientific IRR-P Infrared Temperature Sensor	Side, 1.4m high, 0m out, angled down 45°
CS215 Temperature and Relative Humidity Sensor	Side, 1.8m high, 0.1m out within radiation shield
LI-COR Li 200SA Pyranometer.	Top, 2.3m high, unobstructed

3.3. CIMIS

CIMIS is a system run by the state of California that operates a network of autonomous sensor stations that constantly collect atmospheric and soil data. This data is available for download at cimis.water.ca.gov. The CIMIS data contains variables needed to compute theoretical daily evapotranspiration. This experiment uses the data from the Torrey Pines station, 173, which was tentatively assumed to be near enough Warren field to share atmospheric conditions. Detailed site information on the Torrey Pines station is on the CIMIS website. It shows the station is at least 33m from the nearest building and surrounded by 65m of open turf on three sides. Because it is near Warren, and has similar surroundings, this station might be expected to be representative of Warren evapotranspiration. Daily evapotranspiration is computed from this data for the hours of the data collection and compared to that calculated from the soil samples.

The CIMIS system calculates ET on an hourly basis and sums the results to compute daily and monthly ET. The general version of the Penman-Monteith equation governing ET estimation is discussed in detail in section 2.1.1. The CIMIS website gives elaborate instructions to evaluate a slightly modified version of this equation[3]. The CIMIS website also provides the calculation results with the data.

3.4. Warren Field

Warren Field is roughly 480m x 180m. It is in La Jolla, CA, which enjoys a semi-arid, warm climate. In the month of May, La Jolla averages .61cm of rain, 17.5°C, 70% humidity and 59% sunshine[4]. Warren is primarily Bermuda grass, with a small fraction of perennial rye. Warren is divided into irrigation zones that each are watered four times per week for 30 minutes. Sprinklers put roughly 2.5cm of water on the field each week, though this varies in consideration of rain. Each sprinkler covers roughly a 16m radius circle.

4. Method

4.1. Overview

This study is conducted in three main parts. The first part comprises in-situ sampling of soil moisture and ground temperature to compute ET, and to look in a qualitative and quantitative way for correlations between the two. It

[2] See Appendix A for sensor data

[3] http://wwwcimis.water.ca.gov/cimis/infoEtoCimisEquation.jsp

[4] http://gocalifornia.about.com/cs/sandiego/l/bl_sd_temp.htm

further looks in a qualitative way at the distribution of the ground temperature and soil moisture features. The second part performs statistical analysis to evaluate the most efficient sample spacing for future in-situ measurements. The third part calculates ET from CIMIS data for limited comparison to ET calculations from soil moisture data.

4.2. Data Collection

The extent of the sampling coverage was limited to the westernmost two soccer fields on Warren Field. The data collected is listed in Table 2 and Table 3. Meteorological data was averaged over one minute increments for logging. In-situ data was sampled by the datalogger every two seconds. The in situ data table was switched, so that it logged only while the soil moisture probe was in the ground and giving meaningful output. In situ samples were taken at nodes spaced ten paces (approximately 8m) apart in a square pattern. The intervals of the sampling grid were not carefully controlled, since the data were tied to GPS measurements. The soil probe stabilization is listed by the manufacturer as seven seconds; however testing showed that fluctuation outside the expected error of the probe ceased with two seconds of insertion. At each node the following procedure was executed:

1. Insert soil probe
2. Count five Mississippi
3. Turn on the in-situ table switch
4. Count fifteen Mississippi
5. Turn off the in-situ table switch
6. Remove soil probe
7. Move ten paces

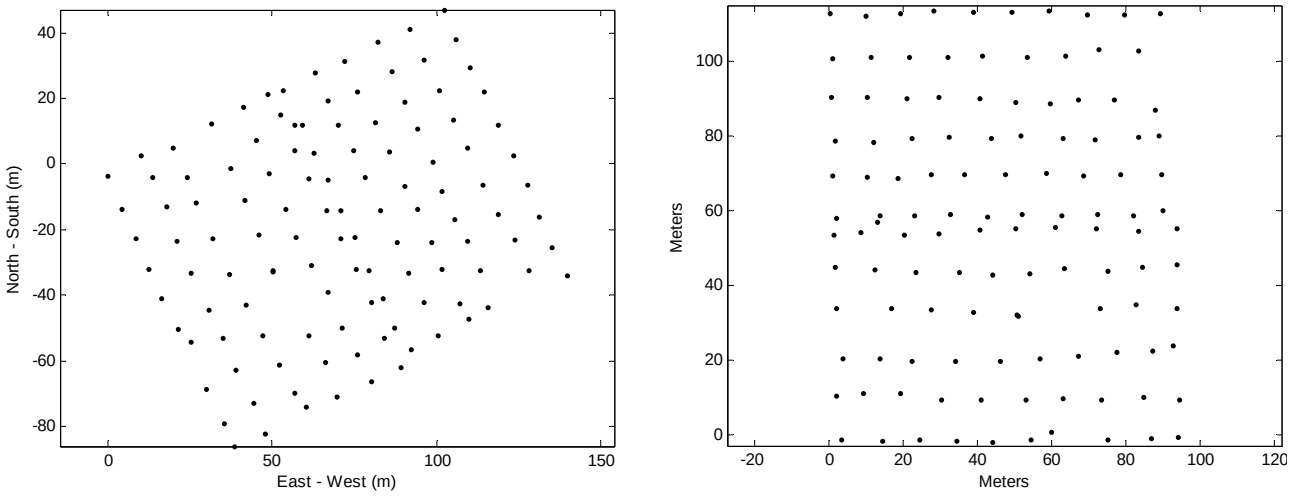

Figure 2. Typical soil sample node spacing. (a) Sample nodes with North at the top. Measurements begin at the leftmost corner and end at the right. Each node is the average of 5-10 samples. (b) Sample nodes rotated for display normal to a reference frame based on the first data point. This is the basis of the distribution figures below. The boundaries of the samples are the out of bounds lines of the soccer fields. The two closely spaced rows in the middle mark the out of bounds lines where the fields meet. Samples taken 25 May, 15:54.

Table 2. Meteorological Data

Measurement	Units	Sensor
Air Temperature	Centigrade	CS-215
Relative Humidity	%	CS-215
Solar Radiation	Watts	Li 200SA
Wind Speed	Meters/s	Davis Wind
Wind Direction	Degrees	Davis Wind

Table 3. In Situ Data

Measurement	Units	Sensor
Soil Probe Voltage Output	Volts	ML2
Soil Volumetric Water Content	%	ML2
Infrared Sensor Ground Temperature	Kelvin	IRR-P
Latitude	Degrees	Garmin GPS
Longitude	Degrees	Garmin GPS
Number of Satellites		Garmin GPS

4.3. Processing of In Situ Measurements

The in situ data collected are logged as tables with the columns indicated by Table 3. They are analyzed by the *Read_insitu_6.m* program. Data processing begins by discarding invalid samples—samples where either the soil voltage probe is not in the ground (arbitrarily specified as less than 0.1 volts), or the GPS has lost satellite contact. Samples are then sorted into bins by sampling node. The measurements at each node are averaged, as are the reported positions, and are saved as vectors. Two vectors are created, one each for ground temperature and volumetric water content. These vectors are interpolated by the MATLAB function *gridfit.m 2.0*, and the results plotted as surfaces.

Latitude and longitude measurements are normalized to the first data point, leaving only fractions of minutes of latitude and longitude. These are converted to meters, using the assumption that the earth is a spheroid, by the following algorithm.

$$R = \sqrt{\frac{\overline{(a*\cos(\varphi))^2 + (b*\sin(\varphi))^2}}{(a*\cos(\varphi))^2 + (b*\sin(\varphi)^2)}}; \tag{7}$$

$$r = R*\cos(\varphi);\ \ x = -r*\sin(long);\ y = R*\sin(lat);$$

where a is the semi major axis at the equator, b is the semi minor axis at the pole, R is the spheroid radius at the point of measurement, φ is the approximate latitude, and r is the radius of the latitude circle at the current latitude. The algorithm outputs x and y—the distances in meters from the first node.

Data processing for semi-variograms creates matrices of the difference between measurements at the i^{th} and j^{th} nodes, and another matrix of the distance between those nodes. These matrices are then sorted into bins based on their distances; e.g., measurements greater than 10m apart but less than or equal to 20m apart go into a single bin, whose distance is reported as 15m.

4.4. Processing of Meteorological Data

In order to calculate local ETo for comparison with CIMIS data, in-situ data must be obtained in the same manner as CIMIS data. CIMIS uses a modified Penman-Monteith equation, the exact steps of which are outlined in Appendix C. The input variables are relative humidity, net radiation, air temperature, wind speed and elevation. The tripod has sensors to collect relative humidity, temperature, and wind speed. The net radiation is borrowed from the CIMIS data. Data for each day were averaged and plugged into the CIMIS Penman equation. The resulting calculated ETo was then compared to CIMIS ETo averaged over the study time intervals.

5. Results

5.1. Meteorological Data

Table 4 shows the variables collected for ET estimation. Table 5 shows the ET calculated from those variables. The left column of Table 5 shows ET for the hours of the study. The second column shows CIMIS reported ET. Since CIMIS reports are not broken down below the hour level, it is not clear how they are being directly compared to in-situ measurements. Because the process of comparison is not known, it is not possible to extend the data out to a daily value for comparison to in-situ measurements—the result would be extremely sensitive to the time periods represented here.

Table 4. Average Variables for ET Calculation

Start time	Temperature (°C)	Relative Humidity (%)	Wind speed (m/s)	Net Radiation[1] (W/m^2)
5/24/2008 07:45	13.61	69.57	0.61	128.00
5/25/2008 16:02	15.68	64.30	2.68	231.67
5/26/2008 13:39	15.85	68.98	2.79	538.00
5/31/2008 15:37	16.56	72.62	2.20	323.33
6/1/2008 15:20	16.82	75.74	1.92	393.50

[1]**Data taken from CIMIS**

Table 5. Comparison of CIMIS and In Situ ET Estimations

ETo (µm)	CIMIS ETo (µm)	Variance (µm)	% Variance
126	120	5.608	4.465
258	253	4.441	1.723
540	547	7.115	1.319
334	333	0.838	0.251
397	395	1.679	0.423

5.2. In Situ Measurements – Volumetric Water Content

Figure 3 shows the mean of volumetric water content over the entire two fields. The first three days, May 24, 25 and 26, show a linear decrease in moisture. The fields were watered early Friday morning, May 23, then not watered again until after the samples on Monday, May 26. During the second weekend, the field was watered in the early morning May 31 and June 1, approximately twelve hours before measurement. These dates show identical soil moisture.

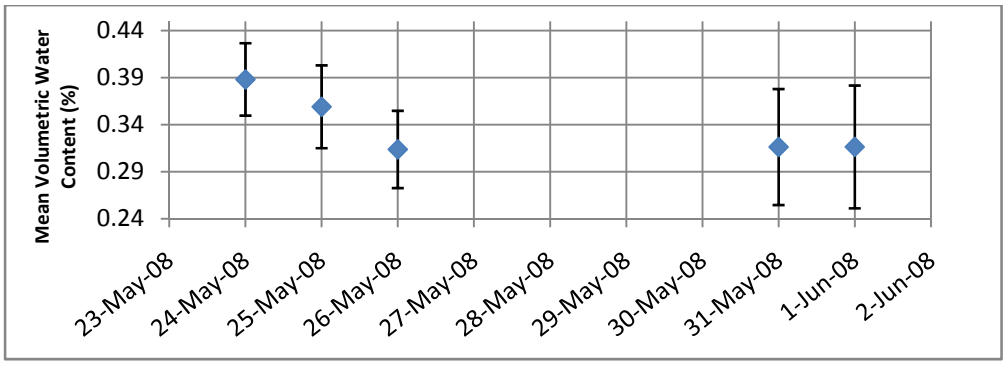

Figure 3. Volumetric water content versus time for the two weekends of the study. VWC decreases linearly over the first weekend while the field is not watered. VWC is constant over the second weekend, as the field was watered each morning before sunrise. The error shown is one standard deviation.

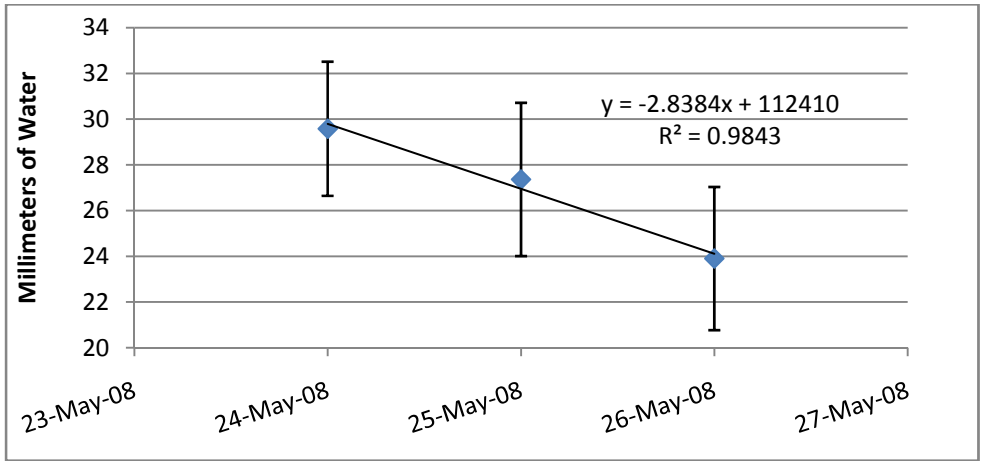

Figure 4. Calculation of millimeters of water for the first weekend of the study. Water height is based on 76.2mm depth multiplied by the volumetric water content from Figure 3. Interpolation shows moisture decreases linearly 2.8mm of water per day. The R^2 value of the interpolation is .984. The error shown is one standard deviation.

Figures 6, 7 and 8 show the water content distribution over the soccer fields during the first weekend. While features are not easily resolvable and inconsistent across days, the general loss of water is apparent, and some broad similarity can be seen. Figures 9 and 10 show the volumetric water content over the second weekend. The fields were watered each day in the early morning, approximately twelve hours prior to sampling. The water content is nearly identical in each. Table 6 illustrates the apparent correlation between the time vector and the data vectors. R is the correlation coefficient. P is the probability of producing the coefficient by random chance.

Table 6. Correlation Coefficients of Time Vector versus Data Vectors, and Between Data Vectors

Day	VWC/ Time R	VWC/ Time P	Ground Temp/ Time R	Ground Temp/ Time P	Ground Temp/ VWC R	Ground Temp/ VWC P
May 24	.2500	.0076	-.1417	.1345	-.0966	.3086
May 25	.2723	.0027	-.8324	0	-.4255	0
May 26	.7537	.0411	-	-	-	-
May 31	.3135	.0004	-.7123	0	-.4360	0
June 1	-.2007	.0300	-.2657	.0038	-.1752	.0588

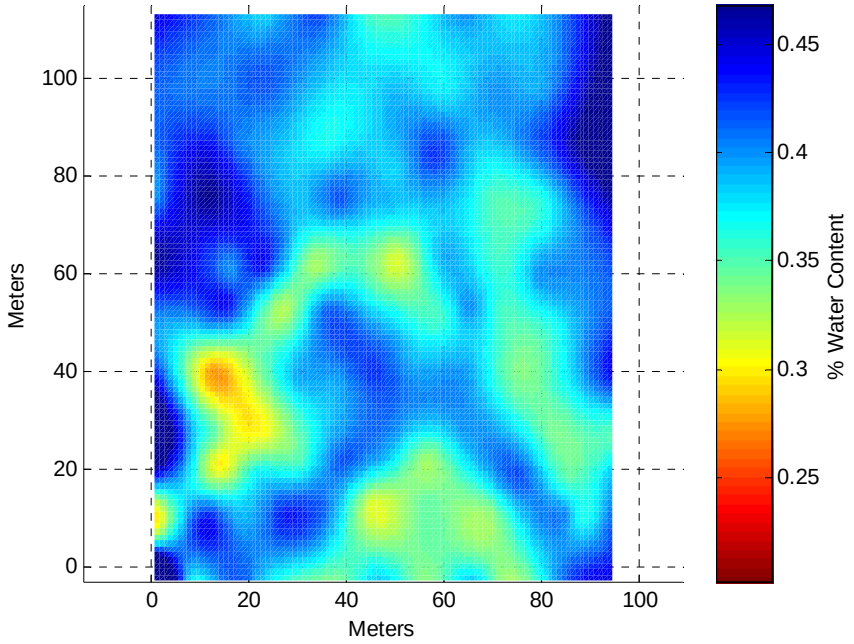

Figure 5. Volumetric water content distribution on the two westernmost Warren soccer fields, 24 May, 7:32. North is the top left corner. The bottom half of the graph comprises a sandy, muddy soccer field; the top half comprises a healthy, grassy field. The aliasing is an artifact of file type conversion. Data was sampled early in the morning, two hours after watering, and water content is very high. The blue area toward the middle is a low, rocky, muddy spot with high water content. The grassy, healthy field has higher water than the more barren field. Minimum observed VWC is 27.6%; maximum is 52.2%; mean is 38.9%.

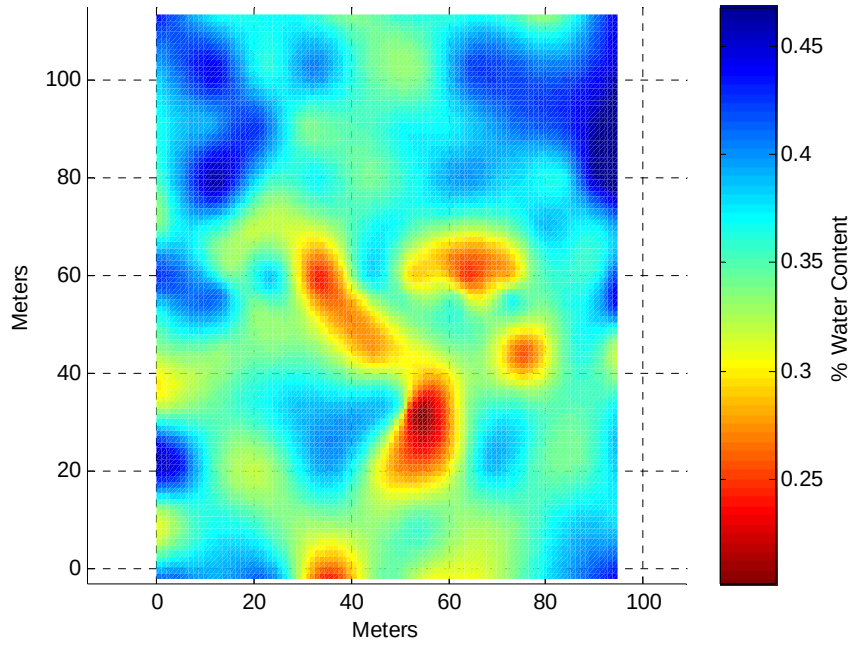

Figure 6. Same as Figure 5, taken 25 May, 15:54. Afternoon data taken on the second day after watering. The high moisture

area in the middle of the barren field has become a very low moisture area. The grassy area of the field is drying more slowly. Minimum observed VWC is 24.2%; maximum is 45.6%; mean is 35.6%.

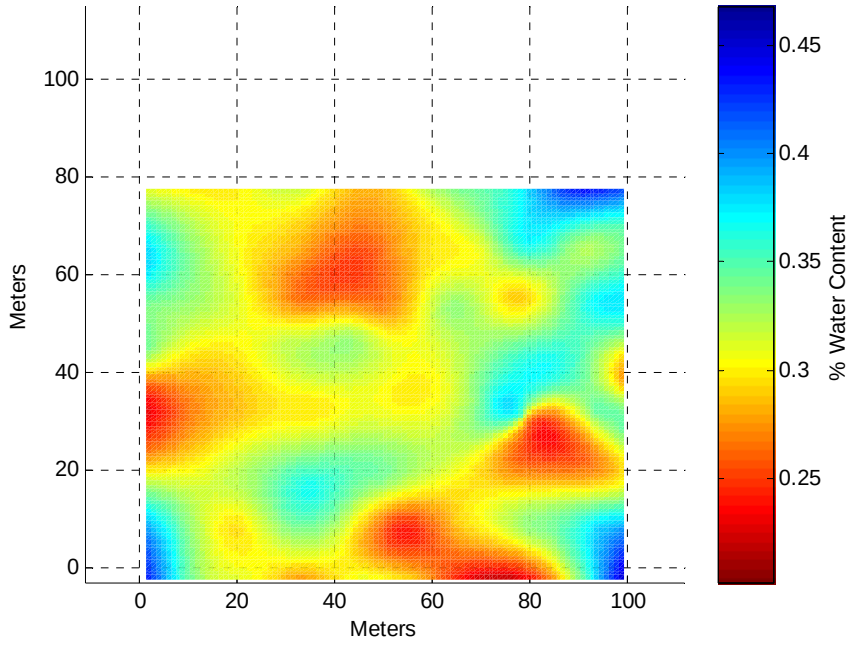

Figure 7. Same as Figure 5, taken 26 May, 13:33. The man taking the data apparently died halfway across the top field. Water content continues to fall. Minimum observed VWC is 22.5%; maximum is 42.5%; mean is 31.4%.

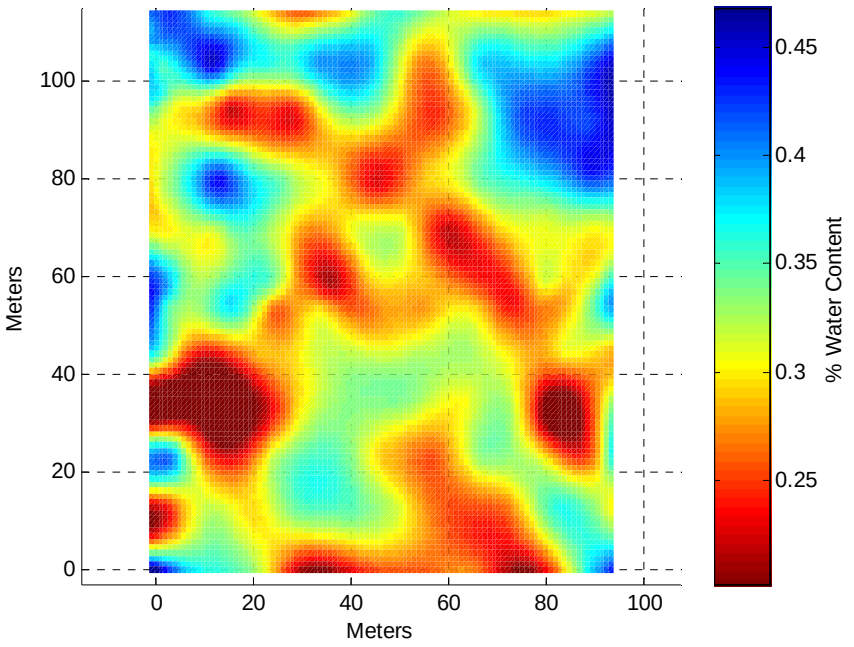

Figure 8. Same as Figure 5, taken 31 May, 15:13. Samples were taken roughly twelve hours after watering, and soil moisture correlates to sprinkler patterns. Water content is as low as the third day after watering the previous week. Minimum

observed VWC is 14.3%; maximum is 44.4%; mean is 31.6%.

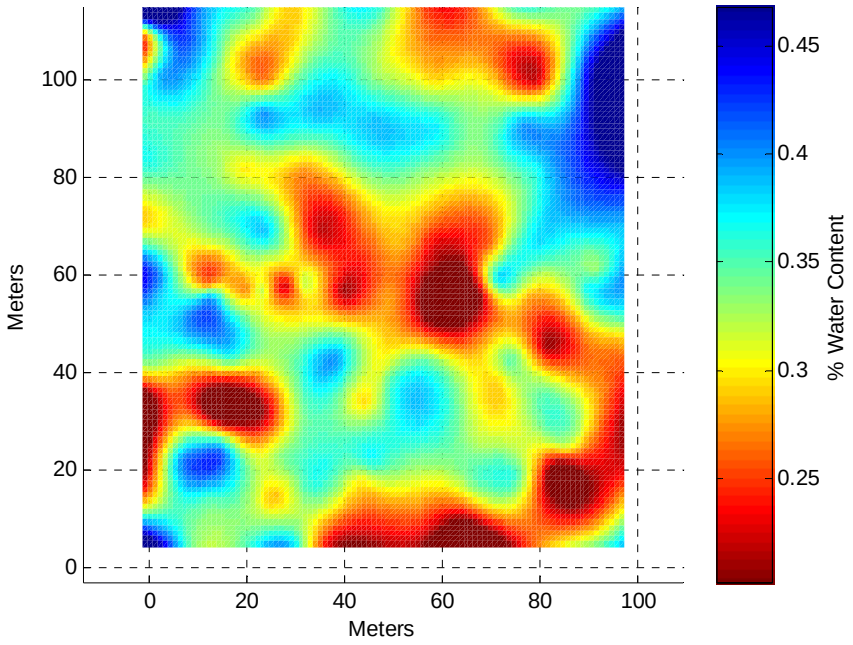

Figure 9. Same as Figure 5, taken 1 June, 15:16. Samples were taken for a second time roughly twelve hours after watering, and soil moisture correlates to sprinkler patterns. Total water content is nearly identical to that of the previous day. While patterns do not overlap dramatically, generally wet and dry spots correlate with those in Figure 8. Minimum observed VWC is 14.5%; maximum is 44.5%; mean is 31.6%.

5.3. In Situ Measurements – Ground Temperature

Figures 11 and 12 show the ground temperature distribution over the first two days of the study, May 24 and 25. Data are not available for May 26. The ground temp on May 24 is almost without feature, as it was taken in the very early morning. The data taken May 25 show the muddy field is significantly warmer than the grassy field. This correlates with the faster drying seen there (Figure 6).

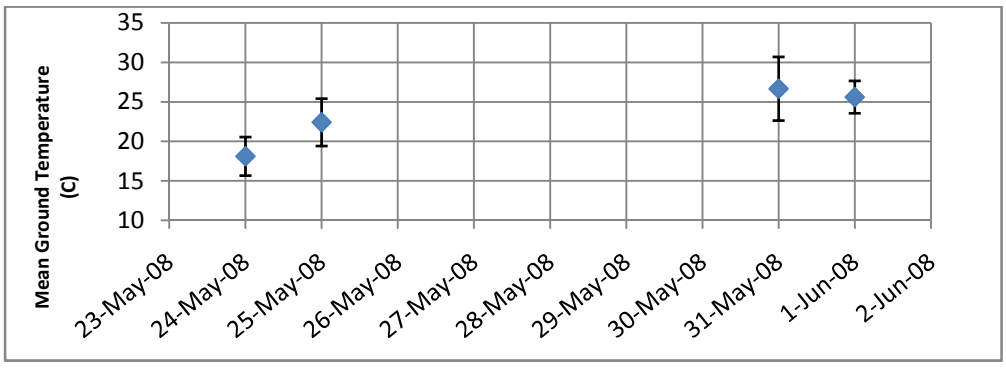

Figure 10. Mean ground temperature for each day. The error shown is one standard deviation. Ground temperature is lowest on 24 May, when data was taken in the early morning. No data is available for 26 May.

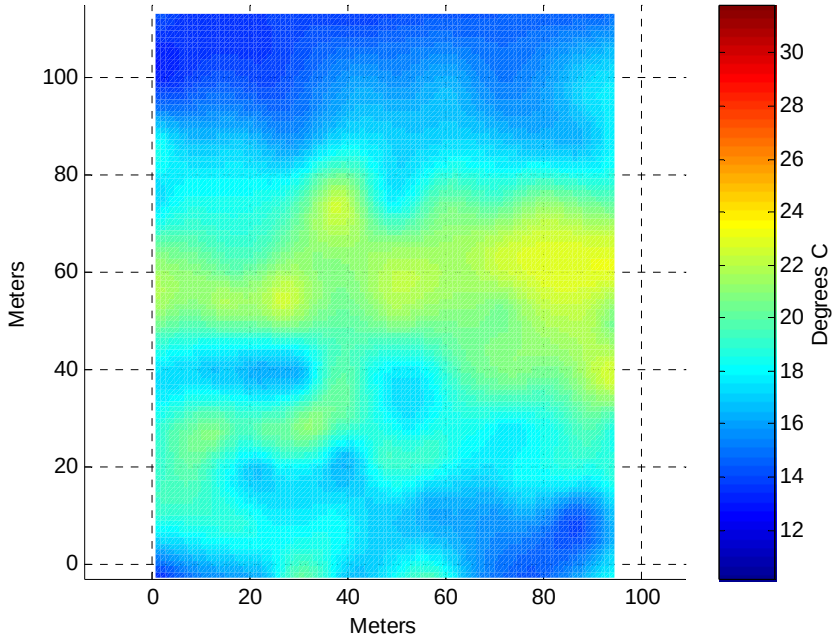

Figure 11. Ground temperature distribution on two westernmost Warren soccer fields, 24 May, 07:32. North is the top left corner. The bottom half of the graph comprises a sandy, muddy soccer field; the top half comprises a healthy, grassy field. The early morning data shows no clear temperature trends. Minimum observed temperature is 15.6 °C; maximum is 23.11 °C; mean is 18.1°C.

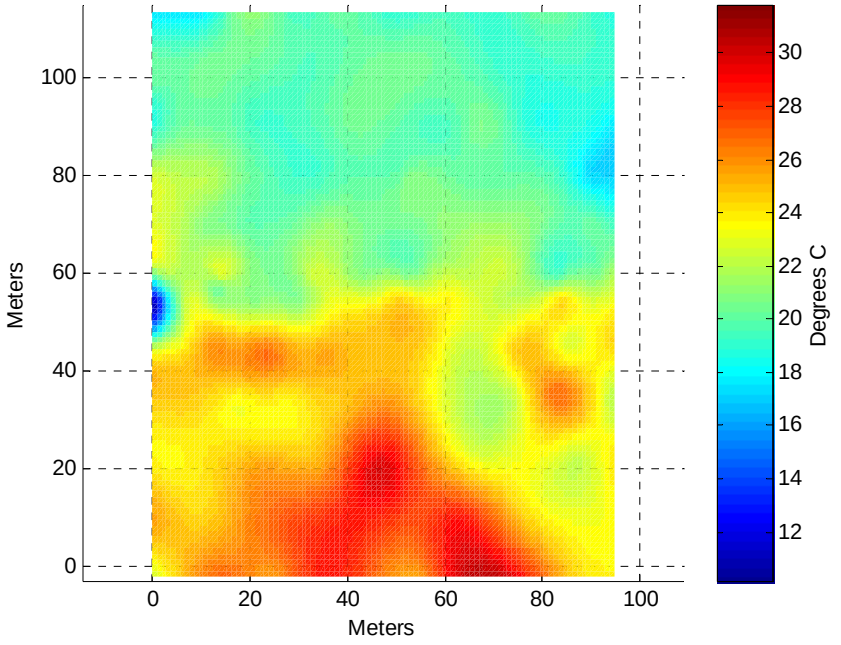

Figure 12. Same as Figure 11, taken 25 May, 15:54. Ground temperature is generally higher in the sandy field, as the data were taken in the afternoon. Minimum observed temperature is 13.6 °C; maximum is 29.9 °C; mean is 22.4°C.

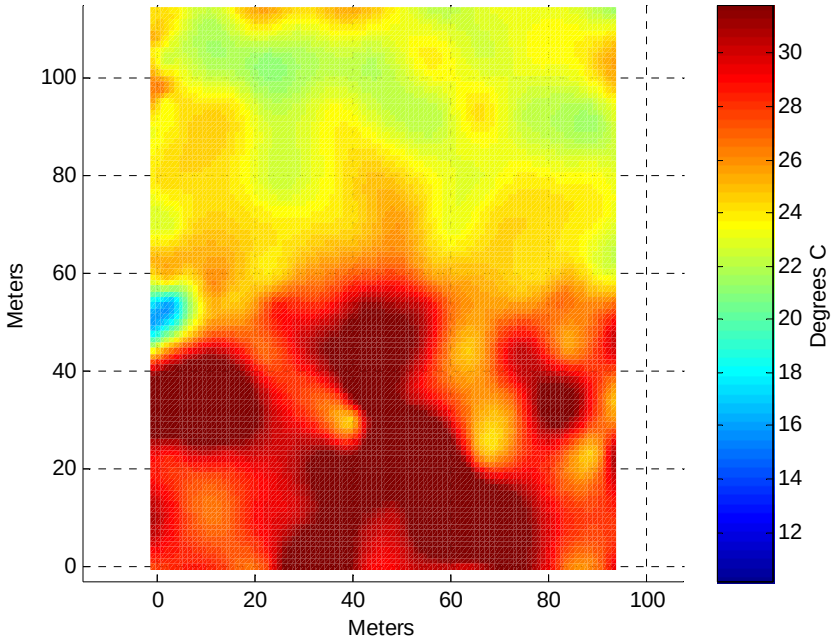

Figure 13. Same as Figure 11, taken 31 May, 15:13. Afternoon data show ground temperature is clearly higher in the sandy field, however the wide range of observed temperatures seem to indicate some defect in the data. Minimum observed temperature is 16.5 °C; maximum is 39.5 °C; mean is 26.7°C.

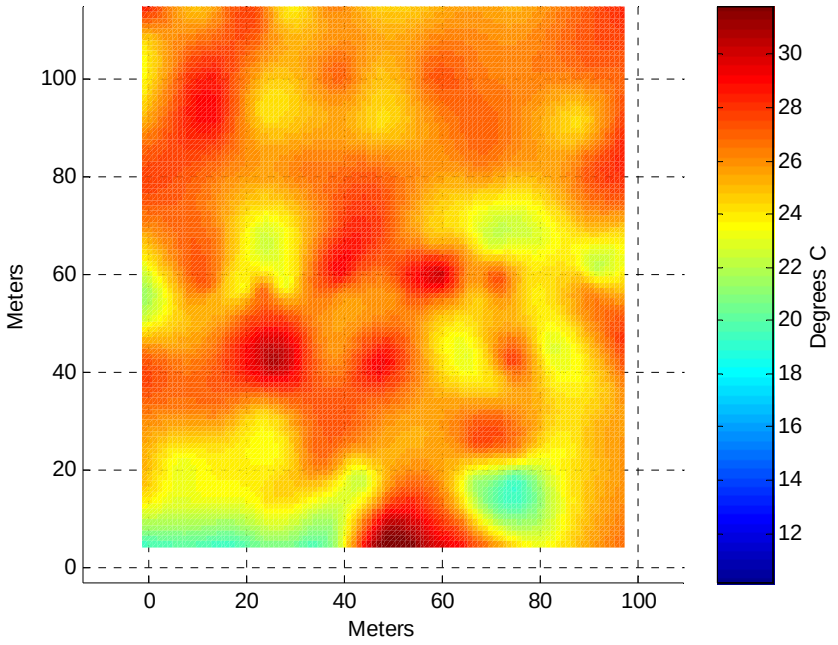

Figure 14. Same as Figure 11, taken 1 June, 15:16. North is the top left corner. Ground temperature is consistent across both fields, which disagrees with the previous two observations. Minimum observed temperature is 19.8 °C; maximum is 30.7 °C; mean is 25.6°C.

5.4. Sample Spacing Analysis

Figures 16-20 show the mean of the semi-variogram plotted versus distance for each unique pair of sampling nodes. Each figure compares Ground temperature and volumetric water content. While there are some differences from plot to plot, water content variance is generally flat as a function of distance. Ground temperature variance generally trends up as a function of distance, though this trend is dominated by the expected error. No clear conclusions could be drawn from directional semi variograms, which are shown in Appendix B

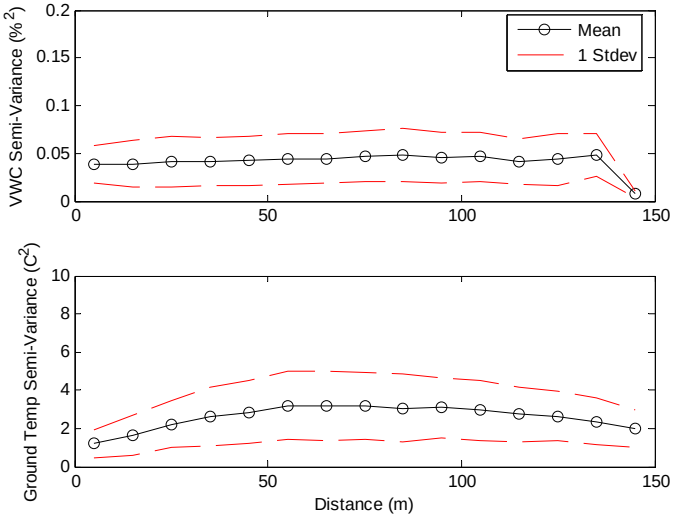

Figure 15. Omni-directional Semi-variograms for Warren Field samples taken 24 May, 07:32. Variances between all possible node pairs are plotted versus distance. Nodes in every direction are plotted together. Circles are the mean measurements at each distance; red dashed lines represent the 68% confidence interval, on standard deviation. VWC variance is steady over the range of the graph with the exception of the dramatic dip at 145m, however the value at 145m represents only one or two node pairs at extreme opposites of the diagonal. Ground temperature variance plateaus at 55m, then drops off slightly. Trends in ground temperature variance are smaller than the expected error.

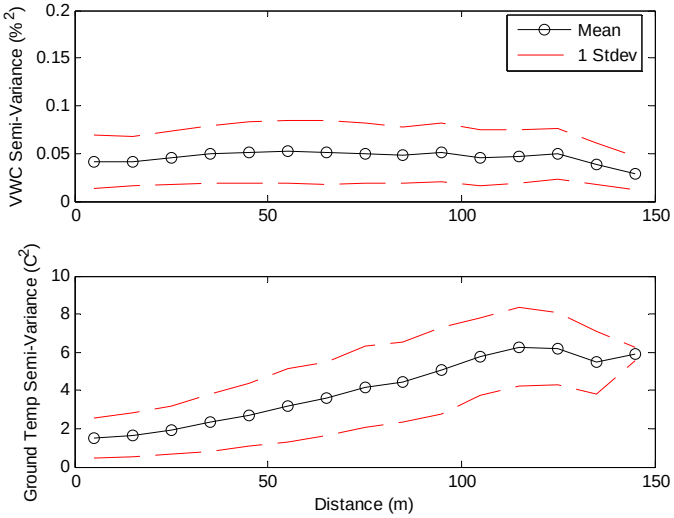

Figure 16. Same as Figure 15, taken 25 May, 15:54. VWC variance is steady over the range of the graph with the exception of a dip at 145m. Ground temp variance rises steadily to an apparent plateau at 115m.

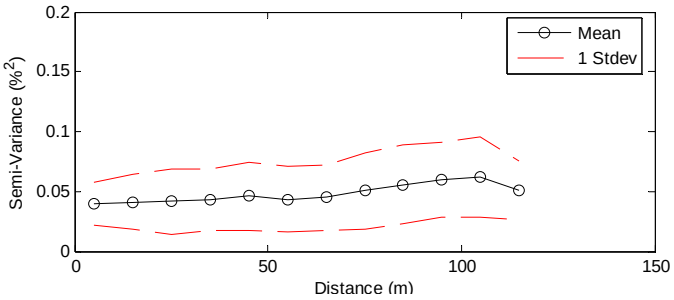

Figure 17. Same as Figure 15, taken 26 May, 13:33. Ground temperature data is not available for this day. VWC variance is steady or climbs very slowly over the range of the graph, though this trend is swamped by the expected error.

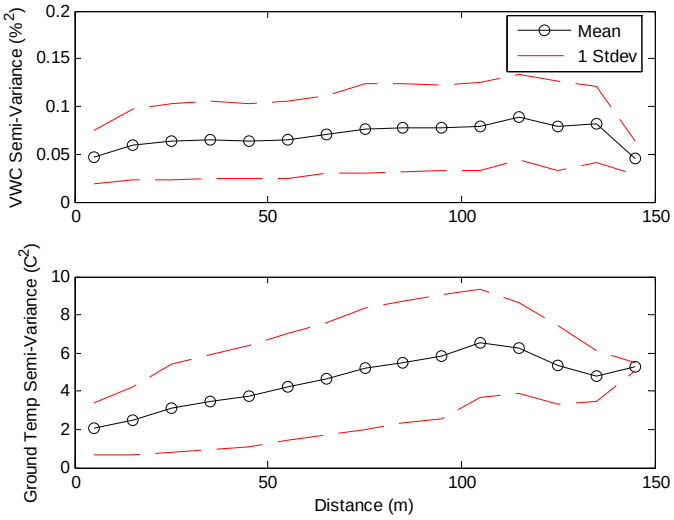

Figure 18. Same as Figure 15, taken 31 May, 15:13. VWC variance is nearly steady as a function of distance. Ground temperature variance climbs to a plateau at 105m.

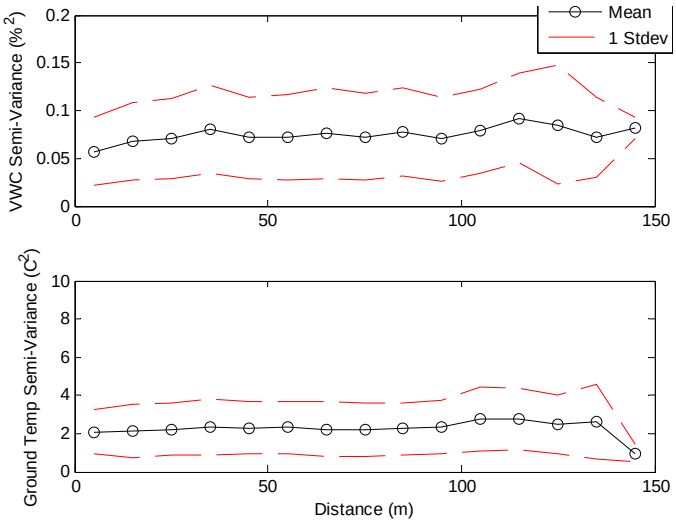

Figure 19. Same as Figure 15, taken 1 Jun, 15:16. VWC variance climbs slowly and unsteadily with distance, dropping off at 135m. Ground temperature variance is nearly steady before dropping at 145m.

5.5. Empirical Check of Sample Spacing

As a check of the results of the semi-variograms, spacing was increased by removing points from the data set. Table 7 shows the results when 1/2 points were removed, followed by 2/3, 3/4. . . 10/11, then finally all but three randomly spaced points. The error is based on three standard deviations. This has the effect of increasing sample spacing, smoothly at first, then increasingly randomly as data points become very rare.

Table 7. Empirical Check of Sample Spacing

N Samples	Mean VWC (%)	Standard Deviation	Mean Ground Temperature (°C)	Standard Deviation
113	39±12	3.85	18±7	2.4
57	38±10	3.33	18±8	2.6
39	40±11	3.71	18±7	2.4
29	39±11	3.80	18±8	2.7
25	39±12	3.91	18±8	2.6
23	39±10	3.19	18±7	2.4
17	40±11	3.72	18±7	2.4
13	38±11	3.51	18±7	2.3
3	42±11	3.66	16±3	1.1

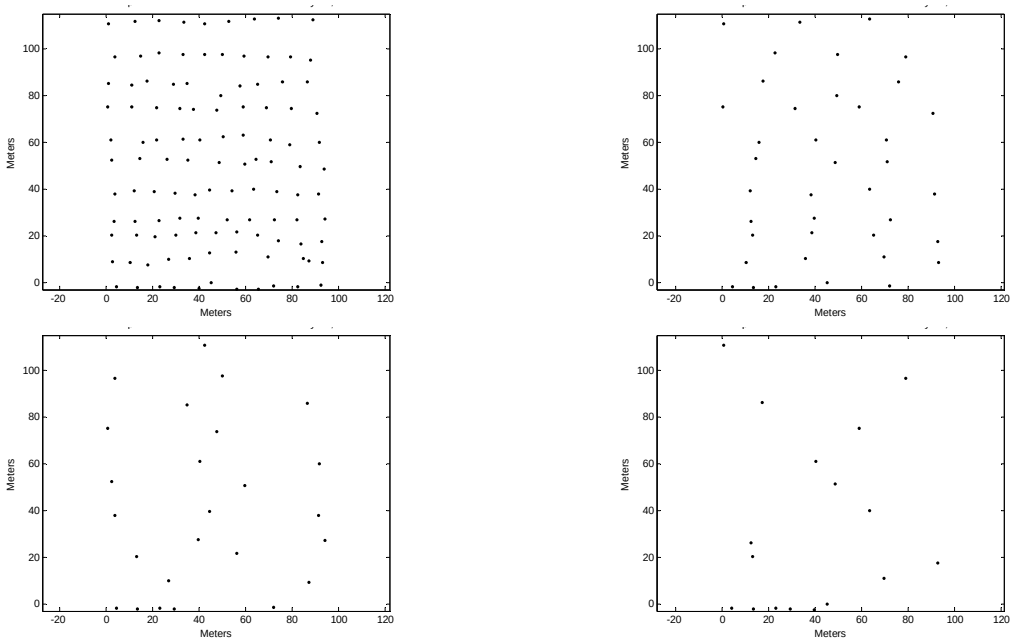

Figure 20. Effect of removing sample nodes. The top left shows 113 nodes. The top right shows 39. The bottom left shows 25 nodes and the bottom right shows 17. The spacing of the nodes becomes increasingly irregular as nodes are removed. The irregularity of the original nodes makes it difficult to remove nodes in a regular manner.

6. Error and Limitations

6.1. Sensor Error

Table 8 shows the expected error associated with each sensor specified by the manufacturer. With the exception of the ThetaProbe, the error of each is small compared to the data. The soil probe error is large; it was compounded by the difficulty of driving it fully into the soil in many cases. Surface temperature measurements were occasionally fouled by people standing in the way of the sensor, the effect of this on the quality of the measurements is not quantifiable. The GPS introduces a position error that is less than one meter. This had no effect on the study.

The approximation used to convert soil probe voltage to soil moisture is valid only to approximately 45-50% VWC. Measurements near this level are suspect.

Table 8. Sensor Error

Sensor	Error	Magnitude WRT data
ML2 ThetaProbe Soil Moisture Sensor	±0.05 m3.m-3	10%
IRR-P Precision Infrared Temperature Sensor	±0.2K	10^{-2}%
Garmin: GPS 16 HVS	Less than 3 meters	1%
LI-200SA Pyranometer	± 5%	
Davis Wind: Anemometer 6410	±1 m/s or ±5%, whichever is greater	
Temperature and Relative Humidity Probe: Model CS215	Temp: ± 4K Hum: ±2.0%	

6.2. Statistical Methods

As discussed in section 2.2.2, geostatistical treatment of the data collected composes a large part of the results, and that information will not be repeated. However, within the semi-variograms, statistical treatment of each bin revealed expected variance that was very large compared to the measurements. While it may seem redundant to treat statistical results statistically, producing a variance variance, it was called for here because of the extremely widely scattered data points in the variance scatter plot (Figure 21). The large confidence intervals generated showed that the trends observed in most semi-variograms were insignificant—swamped by the variance variance. The error shown is only one standard deviation, and is still very large compared to the measurements. This leads directly to one of the study conclusions: that the variance of the i^{th} and j^{th} node does not correlate well with distance.

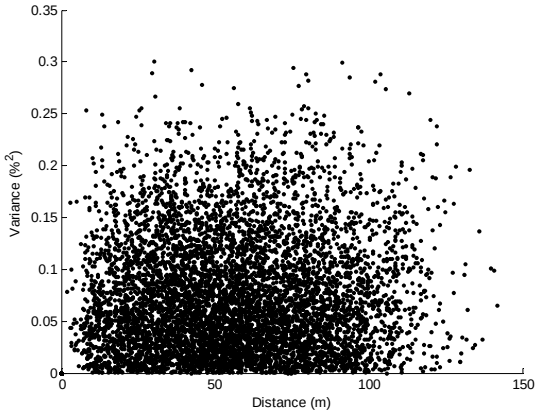

Figure 21. Example scatter plot of semi-variance versus distance. The plot is omni-directional. No trend is apparent. To reveal any trends, the data were sorted into bins to generate semi-variograms; however the clean mean values obscure the chaotic nature of the data. A second level of statistical treatment is required to quantify the variance of the variance.

6.3. Study Limitations

This study was conducted on five days spaced at the most ten days apart. The weather varied little over the period. The miniscule breadth of the study makes it dangerous to draw strong, broad conclusions. Additionally, data is missing. The ground temperature from the third day is omitted because the infrared sensor was never available during that day; and no equipment could be found on what was to be the final day of the study. For the third day again, the data inexplicably ceases in the middle of the top field, perhaps obscuring the developing trend of the top field drying faster than the bottom field. The study is also limited to two soccer fields, while the extent of interest is approximately five times as large. Though the entire extent of Warren field should be homogeneous, that cannot be shown from the data here.

The water content from soil moisture computation is the integration of the soil moisture content as a function of depth from the surface to the depth at which moisture becomes nearly constant. The form of that gradient cannot be determined from the probe here, which is only two inches long. The attempt here to estimate a depth which, under the assumption of constant soil moisture, would yield a curve with the same area as the actual gradient is not precise. This method requires calibration.

7. Discussion

7.1. Soil Moisture and Ground Temperature

The data for the first three days seem to show that the muddy, rocky field is warmer and dries out more quickly than the grassy field. But data in the barren areas is suspect, as mentioned, because the soil probe does not penetrate well there. The ground temperature distribution from the first day (Figure 10) is not meaningful, as the sun is not on the field yet. On day two, the barren side of the field is dryer and warmer. This apparent correlation is confirmed by the coefficients in Table 6, and is repeated on May 31. But it does not directly affect the computation of water loss. Indeed it is not necessary to resolve any features so small in order to accurately compute the mean soil moisture. This correlation between temperature and moisture could not have shown up on May 24, when the early morning ground temperature is constant, nor on May 26, when the data is not available.

Because the measurements were taken across two hours, soil moisture and temperature may have been affected by the time lag. Comparisons of time and data vectors produce significant correlation coefficients (Table 6). However, the measurements began on the generally dryer side of the field. Time induced offset should have gone the opposite direction. This is likely a false correlation based on some intervening variable which is changing with time, or which is changing with position, which in turn changes with time.

The absence of consistent features in the distribution plots is curious. It may be explained by the different rates at which different soil types dry. It is possible the low muddy sandy spots where water pools during irrigation drain more quickly than the grassy areas. It is more likely, though that this is an artifact of the irregular sample pattern. Nodes with high and low measurements will form the peaks and valleys of these charts, and moving the measurement point slightly will skew the presentation though the water pattern does not change. Impractically small lag is required to reliably display any small features of the water and temperature distribution.

7.2. Sample Spacing

The semi-variograms in section 5.4 show clearly that the variance of volumetric water content measurements is not affected by lag. Trends in variance versus distance are overwhelmed by the variance of the variance as shown in the figures there. Variance in ground temperature measurements appears to trend up, especially in Figure 16 and Figure 18; however the error shown there is one standard deviation, where expected error is normally two or three. Coupled with the absence of any trend in the other figures, this indicates ground temperature variance does not depend on distance. Table 7 emphatically verifies these results. Reducing the number of samples taken by a factor of ten introduces a difference of less than 2%. Indeed even reducing the number of samples to three, a statistically meaningless sample size, introduces a difference of only 7%. Taken together, these results indicate that a homogenous area such as Warren Field can be sampled with a very small number of points spaced widely, even up to 100m or more. Both the Geostatistical semi variance and the normally defined standard deviation remain very

small across large distances, as the figures in section 5.4 show.

7.3. Meteorological

The average percent error was only 1.11%. The average total ETo error is calculated to be 0.00109 mm. To make this figure more tangible, it is converted to cubic meters of water wasted over the area of Warren field. The resulting difference between using CIMIS and a local ET station was 0.00774 m^3 of water. This is a negligible amount possibly created by slight fluctuations in air temperature, wind speed or relative humidity. Because the error is so small, however, it is possible that rounding errors in CIMIS data solely responsible for the discrepancy. This is most likely the case, since their hourly average ETo data is rounded to the nearest hundredth. Hence, this experiment clearly shows that there is no need for local ETo measurements at UCSD; the campus climate is well represented by the CIMIS Torrey Pines station.

8. Conclusion

The water lost from the Warren Soccer fields was approximately 2.8mm per day. While the lag in this study was approximately 10m, the data show that volumetric water content for a field approximately 100m by 100m can be reliably calculated from as few as five samples spaced evenly across the diagonal. Soil moisture for the extremely rocky areas of Warren Field is impossible to measure using the probe selected for this study, and the overwhelming source of error is the inability to reliably probe these soils. The water content of these patches is of little interest, moreover, since no desirable plant will take root there.

This study should be repeated over much larger areas, using much wider spacing of samples. The variance of the measurements was large, but had no clear dependence on lag, with the anomalous exception that the variance between the extreme corners of the field was small. Despite the large variance, measurements averaged over the field tend to mean very quickly. Error is strikingly insensitive to number of samples or lag. Homogeneous grassy areas, such as Warren Field, can be reliably sampled for calculation of ET using much larger lags than those in this study. Future studies should also neglect barren, rocky patches of soil in water content measurements. Small features of soil moisture, while interesting to view, are not significant in the computation of total ET and soil moisture. The cost of a sprinkler system that could exploit variations on the scale of 10m would likely be prohibitive. Follow on work should largely ignore this component and focus on comparison of actual water lost to ET estimation from CIMIS and DEMROES data to calibrate ET estimation techniques and to eliminate the need for in-situ measurement. Toward that end, some work should focus on establishing and calibrating an effective depth to approximate the soil moisture gradient. This can be done accurately by using the metered irrigation of Warren Field and comparing it to soil moisture measurements. Attempts to gather this information failed; however it should be readily available. A source of difficulty was the unexpected irrigation of the field during the study. More accurate knowledge of watering times and closer cooperation with grounds crew would improve the value of data.

Given the computed ET of 2.8mm of water, the current irrigation schedule of 2.5cm of water per week is too much for the cool weather during this study. Irrigation should be reduced to 2.0cm of water under these weather conditions, and the soil moisture monitored for verification. Soil moisture monitoring should be less arduous when based on much wider sample spacing.

In order to compare ETo estimation from meteorological data to ETo from in-situ measurement, the estimation must be extended to a daily value, and the crop and stress factors computed. Perhaps future studies could address these complex and vexing problems.

While the data retrieved from this study has limited application due to the very small sample size, it lays the groundwork for much more convenient in-situ measurement of soil moisture. The software written for this study is easily adaptable to any field in the world. Ground temperature measurements may safely be ignored where soil moisture and irrigation schemes are concerned.

9. Assignments and Schedule

Table 9 shows the division of labor for the E3 Experiment.

Table 9. Work Assignment and Schedule

		Week 1	Week 2	Week 3	Week 4	Week 5	Week 6	Week 7	Week 8	Week 9	Week 10
Project Definition	Team										
Research Projects											
Evapotranspiration	Pogue										
Geostatistics	Pogue										
Sensors	Sangel										
Programming											
MATLAB	Pogue/Sangel										
BASIC	Pogue/Sangel										
Wheel Mount	Sangel										
Midterm Report	Pogue										
In Situ Measurements	Team										
Data Evaluation											
Soil Moisture	Pogue/Sangel										
Ground Temp	Pogue/Keller										
Meteorological	Kromsky										
Movie	Keller										
Final Report											
Front Matter	Pogue/										
Method	Pogue										
Setup	Pogue/Keller										
Soil Moisture	Pogue/Sangel										
Ground Temp	Pogue/Sangel										
Meteorological	Kromsky										
Error	Pogue										
Conclusion	Pogue										
Edit	Pogue										
Appendices	Sangel										

References

Clarke, I., 1979. Practical Geostatistics

Western, A.W., 1999. On the Spatial Scaling of Soil Moisture. Journal of Hydrology 217, 203–224.

Famiglietti, J. S., Devereaux, J. A., Laymon, C. A., Tsegaye, T., Houser, P. R., Jackson, T. J., Graham, S. T., Rodell, M., van Oevelen, P.J., 1999. Ground-based investigation of soil moisture variability within remote sensing footprints during the Southern Great Plains 1997 (SGP97) Hydrology Experiment. Water Resources Research 35, 1839-1851.

Ryu, D., Famiglietti, J. S., 2006. Multi-Scale Spatial Correlation and Scaling Behavior of Surface Soil Moisture. Geophysical Research Letters 33.

Bertuzzi, P., Bruckler, L., Bay, D., Chanzy, A., 1994. Sampling Strategies for Soil Water Content to Estimate Evapotranspiration. Irrigation Science 14, 105-115.

Rodriguez-Iturbe, I., Vogel, G.K., Riggon, R., Entkhabi, D., Castelli, F., Rinaldo, A., 1995. On the Spatial Organization of Soil Moisture Fields. Geophysical Research Letters, 22, 2757-2760.

Allen, R.G., Pereira, L.S., Raes, D., Smith, M. 1998. Crop Evapotranspiration - Guidelines for Computing Crop Water Requirements - FAO Irrigation and Drainage Paper 56. Food and Agriculture Organization of the United Nations.

Appendix A – Sensor Data

A.1 ML2 ThetaProbe Soil Moisture Sensor

ftp://ftp.dynamax.com/Manuals/ml2x.pdf

This sensor works by using four sharpened stainless steel rods, inserted in the soil, to apply a 100 MHz sinusoidal signal to the soil. The impedance of this signal varies with the impedance of the soil, which is dependent on its dielectric constant and ionic conductivity. The 100 MHz signal minimizes the influence of the ionic conductivity leaving the impedance dependent of the dielectric constant. Since the soils dielectric constant is almost negligible compared to that of water, the impedance varies mainly with the water content of the soil. The sensor outputs an analogue voltage proportional to the impedance of the signal giving a VMC reading. *Units- % or m^3/m^3*

Figure A-1. Soil Moisture Sensor

A.2 IRR-P Precision Infrared Temperature Sensor

http://www.campbellsci.com/irr-p

This sensor works by measuring the infrared radiation being emitted by the target without touching it, giving the surface temperature. With the use of a thermopile, the temperature difference between the target and sensor body can be measured with a millivolt output. The sensor body temperature is used to reference the target. *Units- Degrees*

Figure A-2. IR Temperature Sensor

A.3 Garmin: GPS 16 HVS

http://www.campbellsci.com/documents/manuals/gps16-hvs.pdf

This sensor works by communicating with up to twelve satellites at a time and determining its distance to each. Using this information, it uses trilateration to deduce its own location. *Units- Longitude and Latitude*

Figure A-3. Garmin GPS 16 HVS

A.4 LI-200SA Pyranometer

http://www.licor.com/env/PDF_Files/200.pdf

This sensor works by using a silicon photovoltaic detector to detect solar radiation. The sensor has a current output which is directly proportional to solar radiation. *Units- W/m^2*

Figure A-4. LI-200SA Pyranometer

A.5 Davis Wind: Anemometer 6410

http://www.davisnet.com/product_documents/weather/spec_sheets/6410_Spec_Rev_E.pdf

This sensor works by using a fin orientate itself in the direction of the breeze. To determine speed it has rotating cups that move with the wind. The rotational speed is then converted to linear speed. *Units- degrees and m/s*

Figure A-5. Davis Wind Anemometer

A.6 Temperature and Relative Humidity Probe: Model CS215

http://www.campbellsci.com/documents/lit/b_cs215.pdf

http://www.sensirion.com/en/pdf/product_information/Data_Sheet_humidity_sensor_SHT1x_SHT7x_E.pdf

This sensor works by using a capacitive polymer sensing element for relative humidity and a bandgap temperature sensor. When exposed to sunlight, the sensor uses a 41303-5A radiation shield to block it from the sun. It uses a digital output. *Units- % RH and Degrees*

Figure A-6. **Temperature and Relative Humidity Probe: Model CS215**

Appendix B – Directional Semi-Variograms

It was concluded as expected that variance in ground temperature and soil moisture was independent of direction. The directional semi-variograms below show ground temperature or soil moisture semi-variograms plotted versus distance. They show no clear trends, and are presented without further comment.

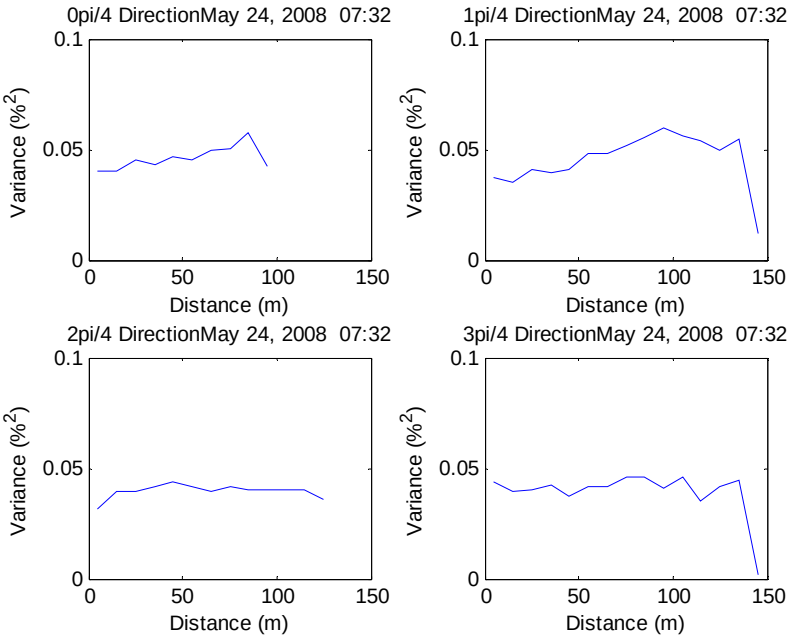

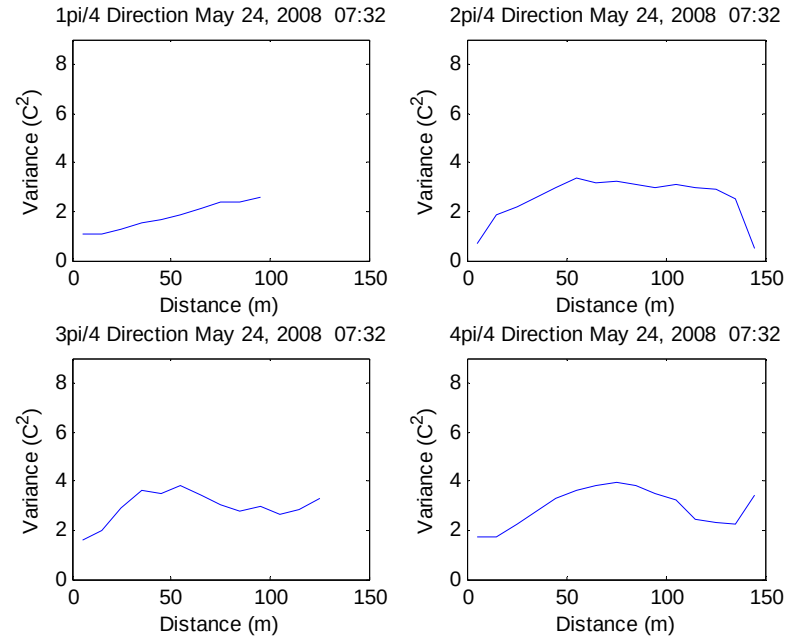

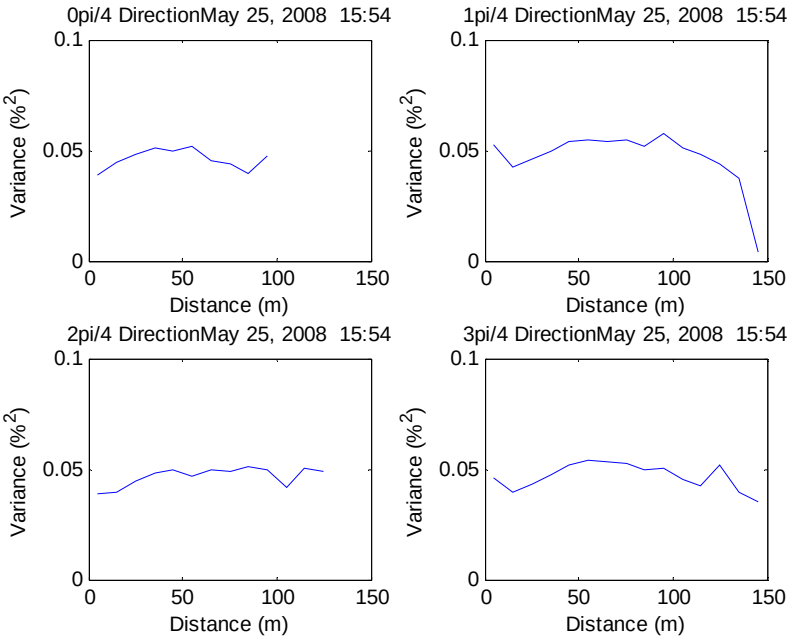
0pi/4 DirectionMay 25, 2008 15:54
1pi/4 DirectionMay 25, 2008 15:54
2pi/4 DirectionMay 25, 2008 15:54
3pi/4 DirectionMay 25, 2008 15:54
Variance (%2)
Distance (m)
0
0.05
0.1
0
50
100
150

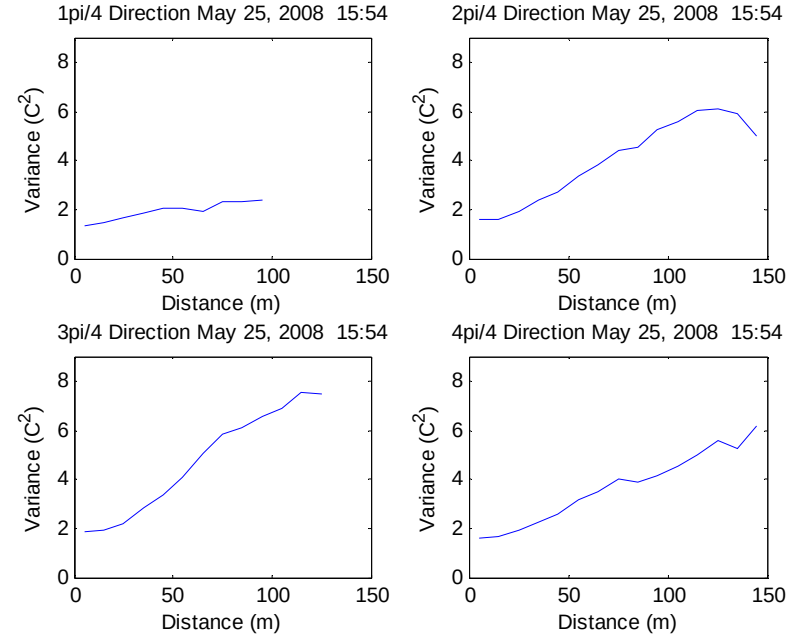
1pi/4 Direction May 25, 2008 15:54
2pi/4 Direction May 25, 2008 15:54
3pi/4 Direction May 25, 2008 15:54
4pi/4 Direction May 25, 2008 15:54
Variance (C2)
Distance (m)
0
2
4
6
8
0
50
100
150

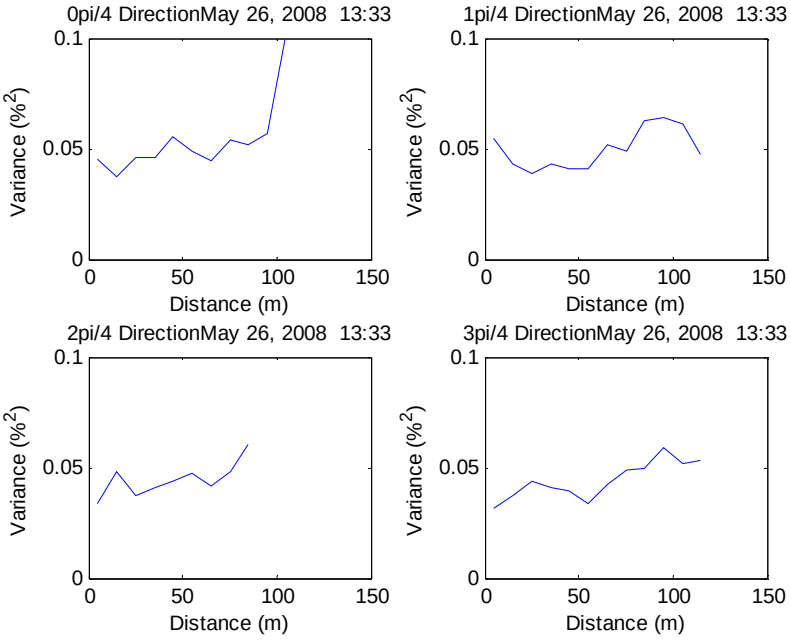
0pi/4 DirectionMay 26, 2008 13:33
1pi/4 DirectionMay 26, 2008 13:33
2pi/4 DirectionMay 26, 2008 13:33
3pi/4 DirectionMay 26, 2008 13:33
Variance (%2)
Distance (m)
0
0.05
0.1
0
50
100
150

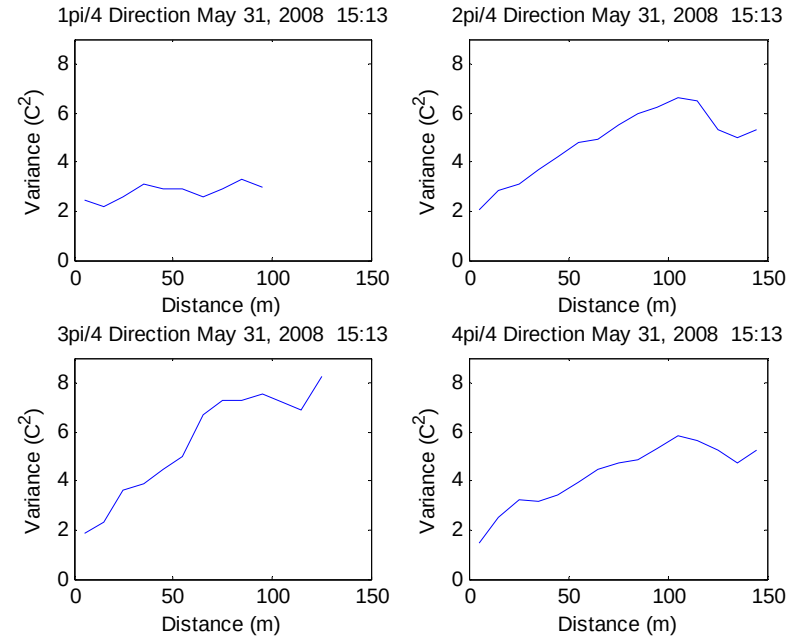
1pi/4 Direction May 31, 2008 15:13
2pi/4 Direction May 31, 2008 15:13
3pi/4 Direction May 31, 2008 15:13
4pi/4 Direction May 31, 2008 15:13
Variance (C2)
Distance (m)
0
2
4
6
8
0
50
100
150

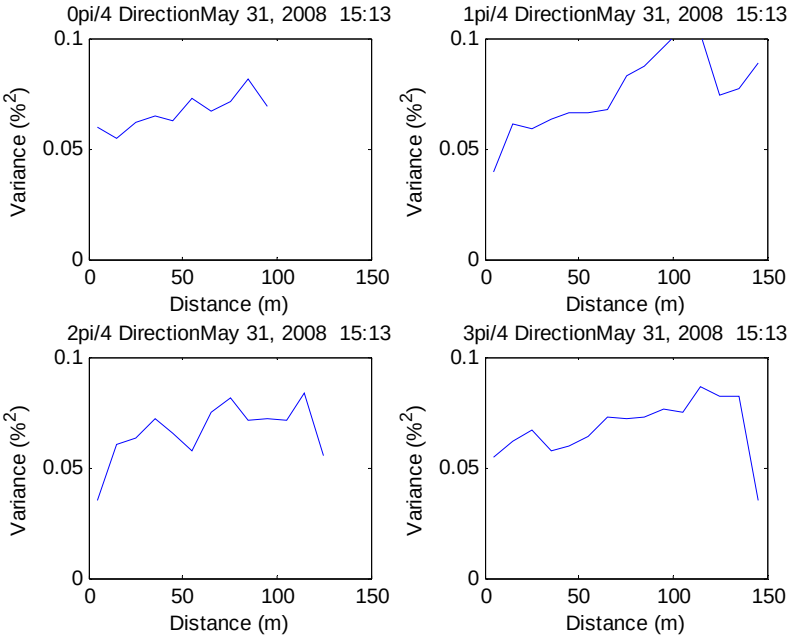
0pi/4 DirectionMay 31, 2008 15:13
1pi/4 DirectionMay 31, 2008 15:13
2pi/4 DirectionMay 31, 2008 15:13
3pi/4 DirectionMay 31, 2008 15:13
Variance (%2)
Distance (m)
0
0.05
0.1
0
50
100
150

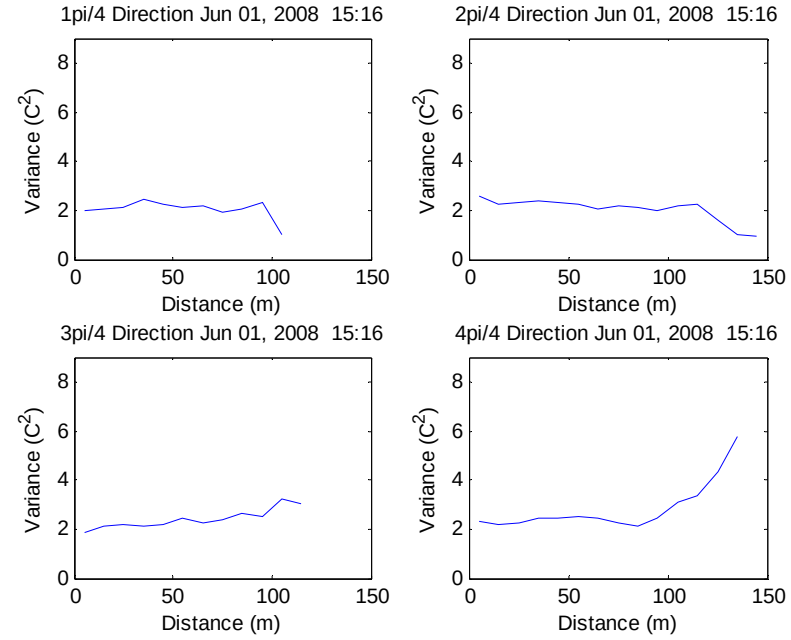
1pi/4 Direction Jun 01, 2008 15:16
2pi/4 Direction Jun 01, 2008 15:16
3pi/4 Direction Jun 01, 2008 15:16
4pi/4 Direction Jun 01, 2008 15:16
Variance (C2)
Distance (m)
0
2
4
6
8
0
50
100
150

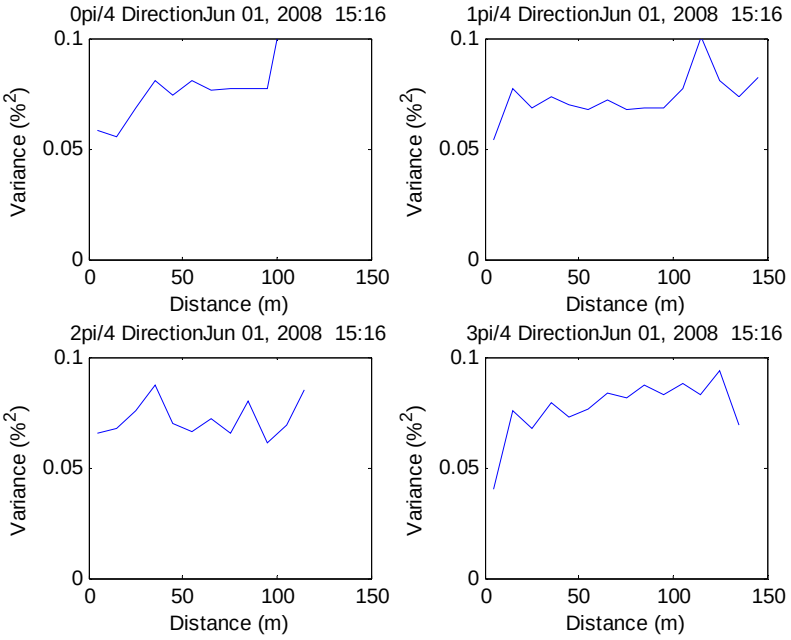
0pi/4 DirectionJun 01, 2008 15:16
1pi/4 DirectionJun 01, 2008 15:16
2pi/4 DirectionJun 01, 2008 15:16
3pi/4 DirectionJun 01, 2008 15:16
Variance (%2)
Distance (m)
0
0.05
0.1
0
50
100
150

Appendix C – CIMIS Modified Penman Monteith

Refer to http://wwwcimis.water.ca.gov/cimis/infoEtoCimisEquation.jsp

Variables Required

RH = relative humidity [%]

Rn = net radiation [Wm^{-2}]

T = air temperature [Celsius]

U = wind speed at 2 meters [ms^{-1}]

Z = Elevation of the station above mean sea level [m]

Steps

1. **Saturation vapor pressure** es = 0.6108 * exp(T * 17.27/ (T + 237.3))
2. **Convert relative humidity to vapor pressure** ea = RH*es/100
3. **VPD - Vapor pressure deficit** VPD = es - ea (kPa)
4. **DEL - Slope of the saturation vapor pressure vs. air temperature curve at the average hourly air temperature**

   DEL = (4099 * es)/$(T + 237.3)^2$
5. **Barometric pressure** P = 101.3 - 0.0115 * Z + 5.44 * 10^{-7} * Z^2
6. **GAM - Psychrometer constant (kPa C^{-1})** GAM = 0.000646 (1 + 0.000946*T) P
7. **W - Weighting function** W = DEL/(DEL + GAM)
8. **FU2 - Wind function**
   For Rn>0 (daytime)
   FU2 = 0.030 + 0.0576U
9. **NR - Convert Rn from Wm^{-2} to mm** NR = Rn/(694.5 (1-0.000946*T))
10. **Hourly ETo is approximately equal to RET** RET = W*NR + (1-W)VPD * FU2

Appendix D – Lesser Meteorological Data

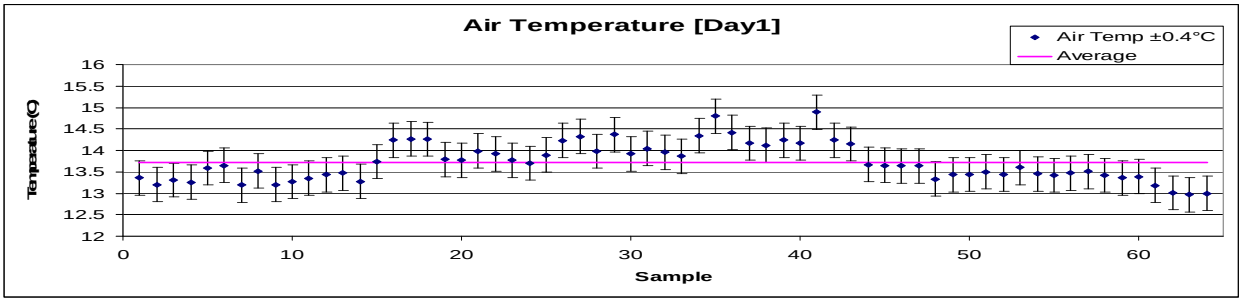

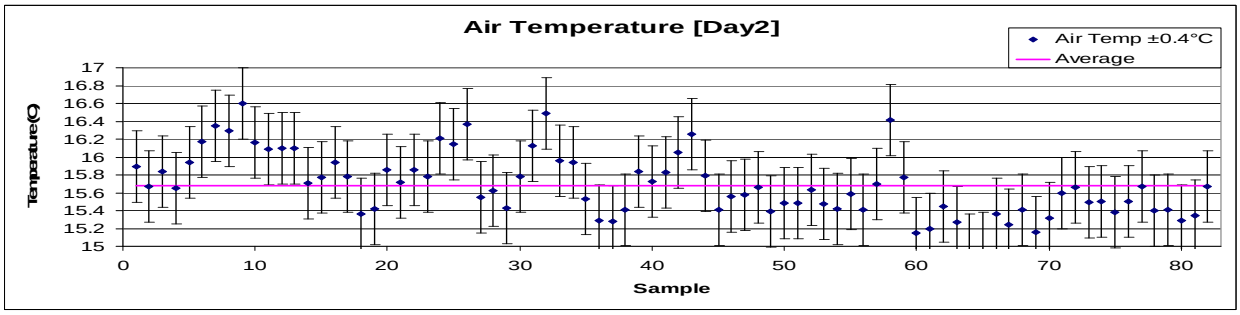

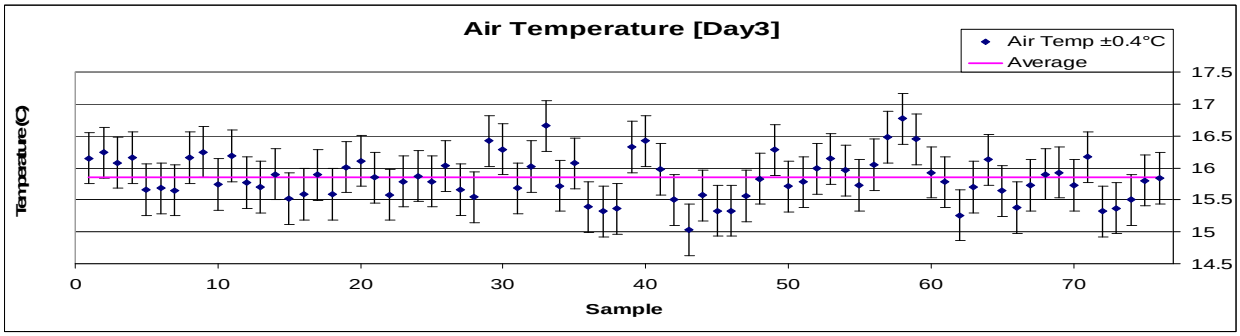

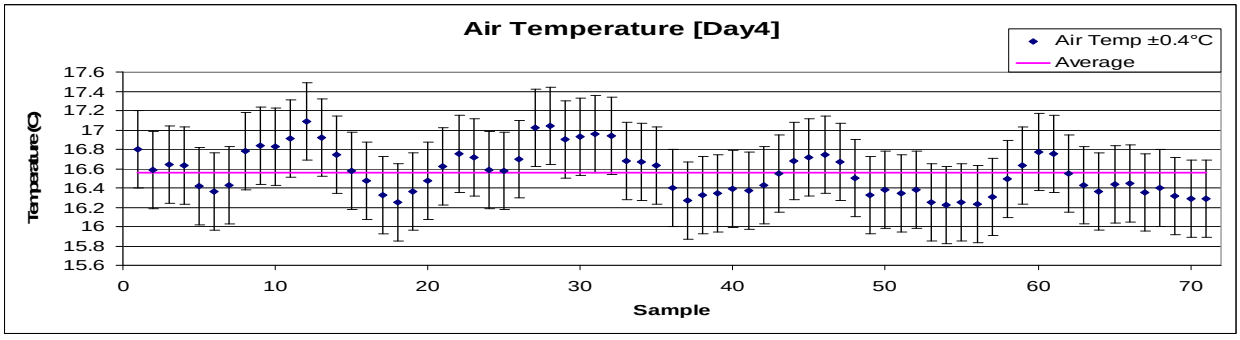

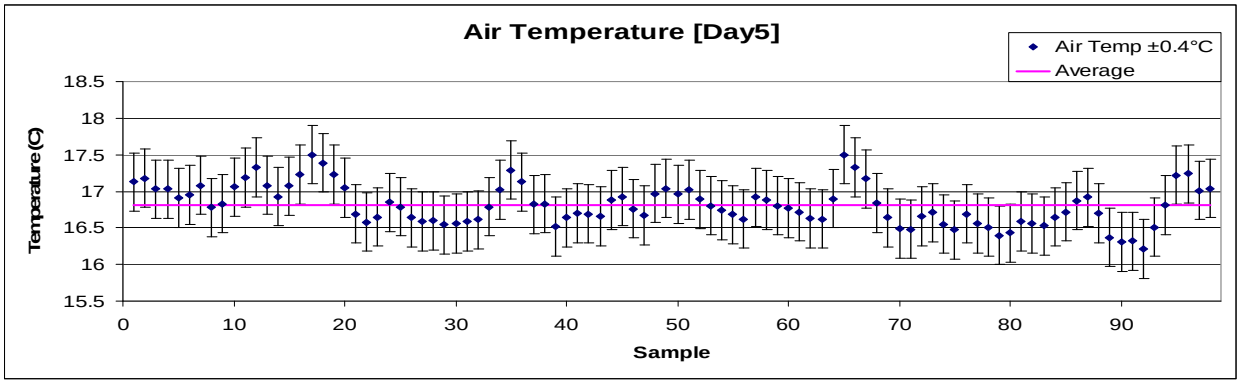
Air Temperature [Day5]
Air Temp ±0.4°C
Average
Temperature (C)
18.5
18
17.5
17
16.5
16
15.5
0
10
20
30
40
50
60
70
80
90
Sample

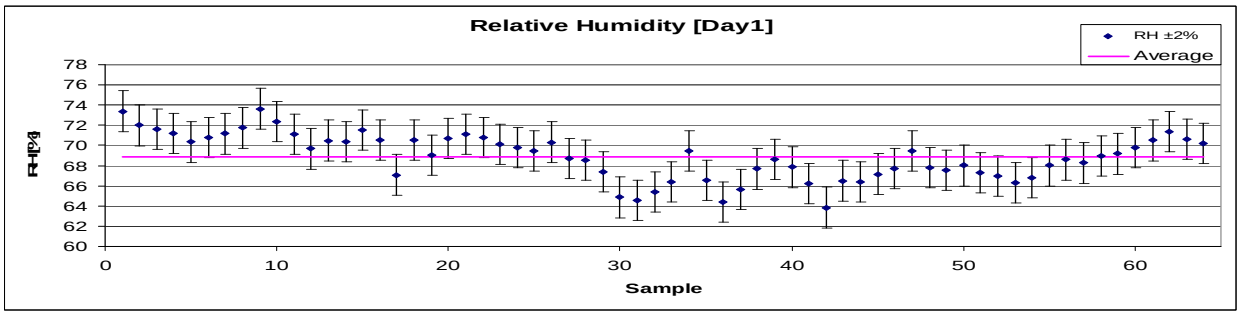
Relative Humidity [Day1]
RH ±2%
Average
RH (%)
78
76
74
72
70
68
66
64
62
60
0
10
20
30
40
50
60
Sample

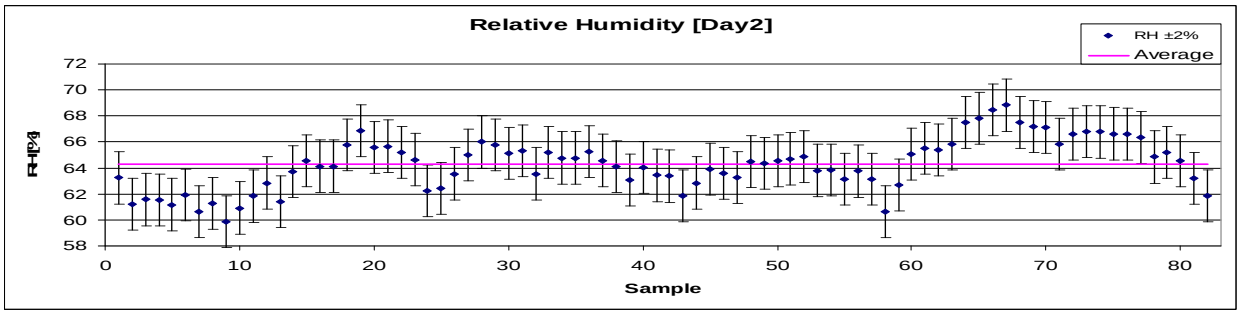
Relative Humidity [Day2]
RH ±2%
Average
RH (%)
72
70
68
66
64
62
60
58
0
10
20
30
40
50
60
70
80
Sample

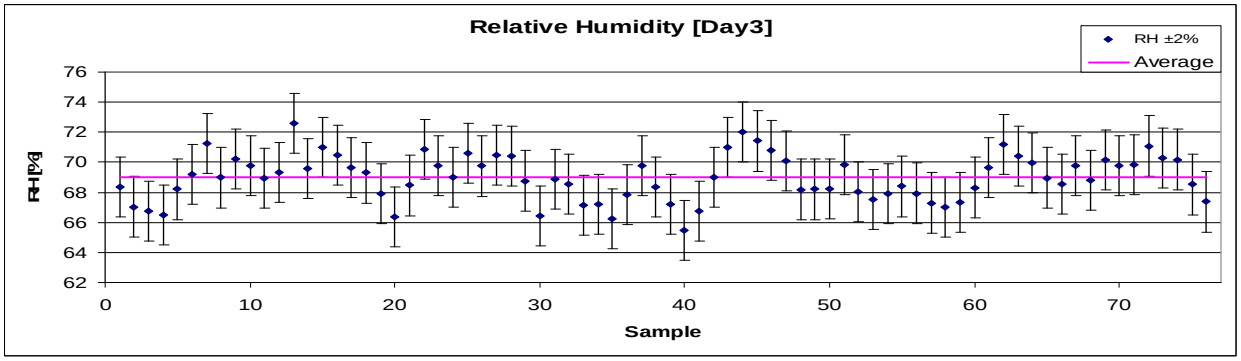
Relative Humidity [Day3]
RH ±2%
Average
RH (%)
76
74
72
70
68
66
64
62
0
10
20
30
40
50
60
70
Sample

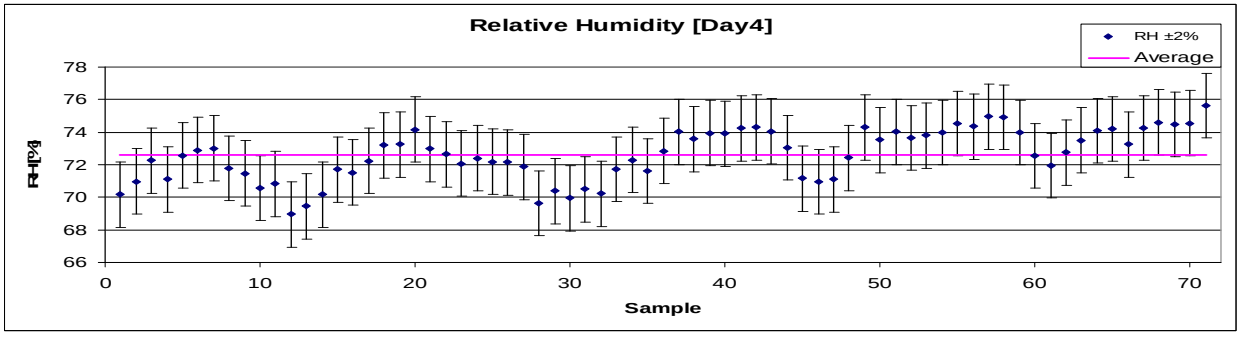
Relative Humidity [Day4]
RH ±2%
Average
RH (%)
78
76
74
72
70
68
66
0
10
20
30
40
50
60
70
Sample

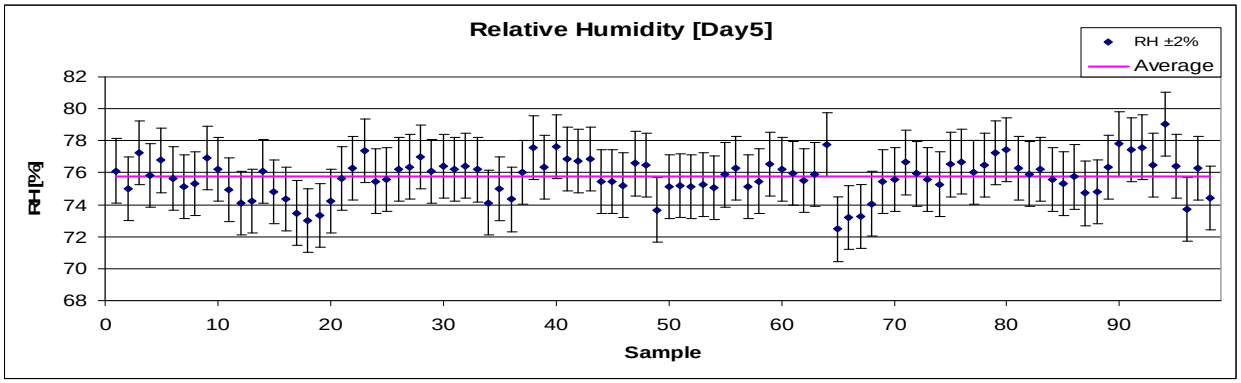
Relative Humidity [Day5]
RH ±2%
Average
RH[%]
82
80
78
76
74
72
70
68
0
10
20
30
40
50
60
70
80
90
Sample

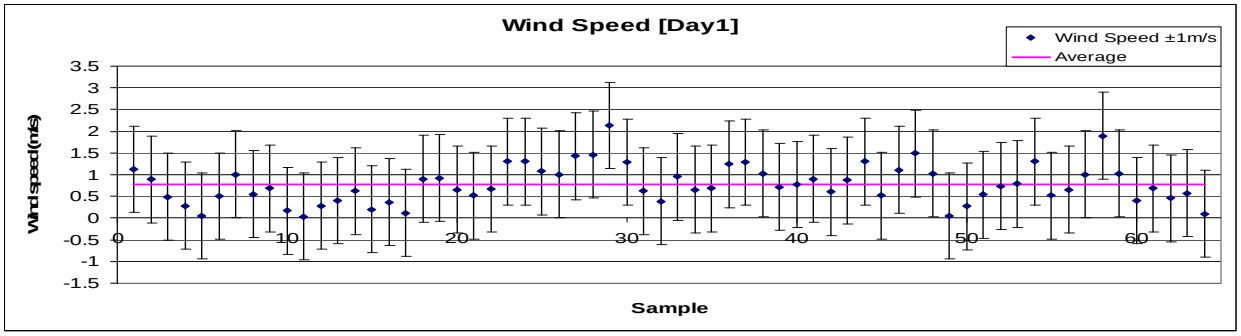
Wind Speed [Day1]
Wind Speed ±1m/s
Average
Wind speed (m/s)
3.5
3
2.5
2
1.5
1
0.5
0
-0.5
-1
-1.5
0
10
20
30
40
50
60
Sample

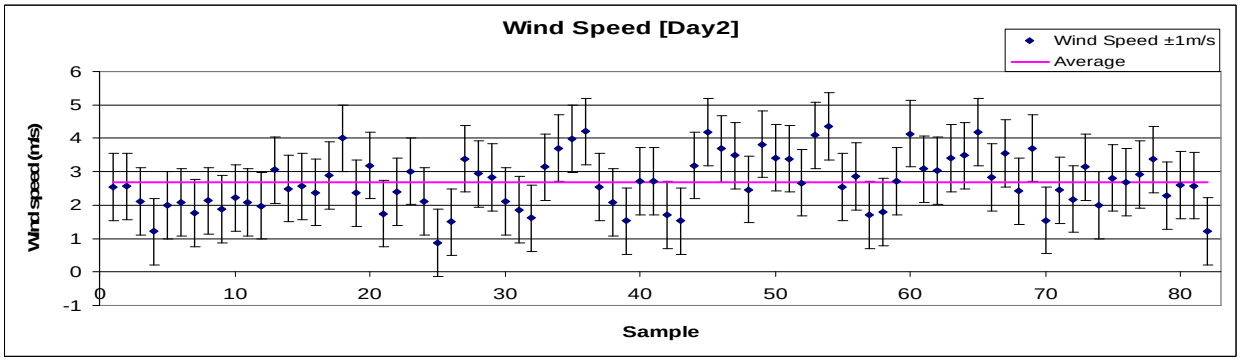
Wind Speed [Day2]
Wind Speed ±1m/s
Average
Wind speed (m/s)
6
5
4
3
2
1
0
-1
0
10
20
30
40
50
60
70
80
Sample

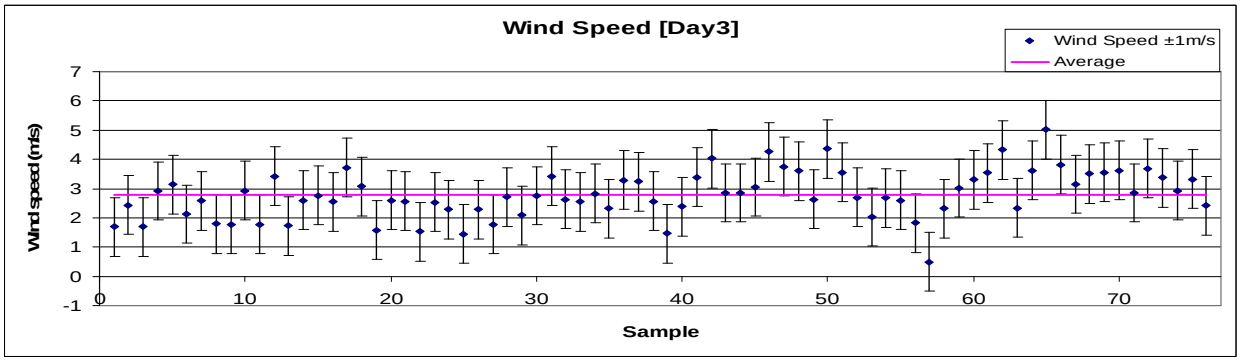
Wind Speed [Day3]
Wind Speed ±1m/s
Average
Wind speed (m/s)
7
6
5
4
3
2
1
0
-1
0
10
20
30
40
50
60
70
Sample

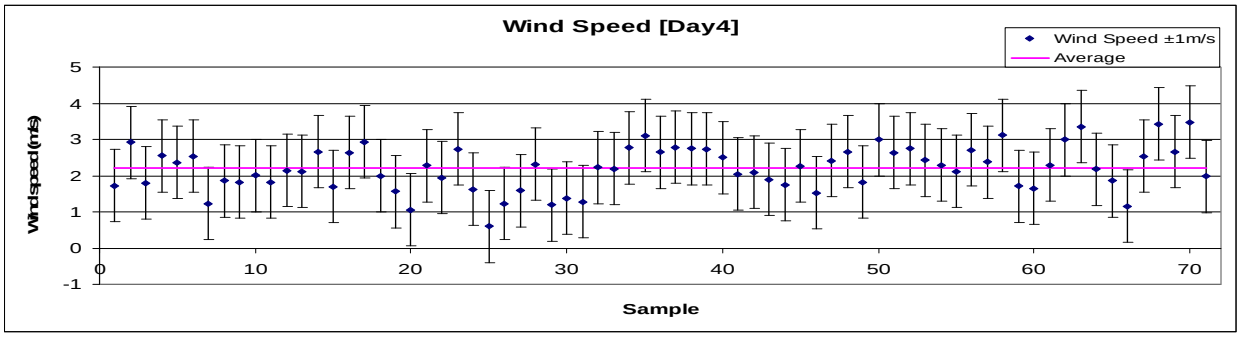
Wind Speed [Day4]
Wind Speed ±1m/s
Average
Windspeed(m/s)
5
4
3
2
1
0
-1
0
10
20
30
40
50
60
70
Sample

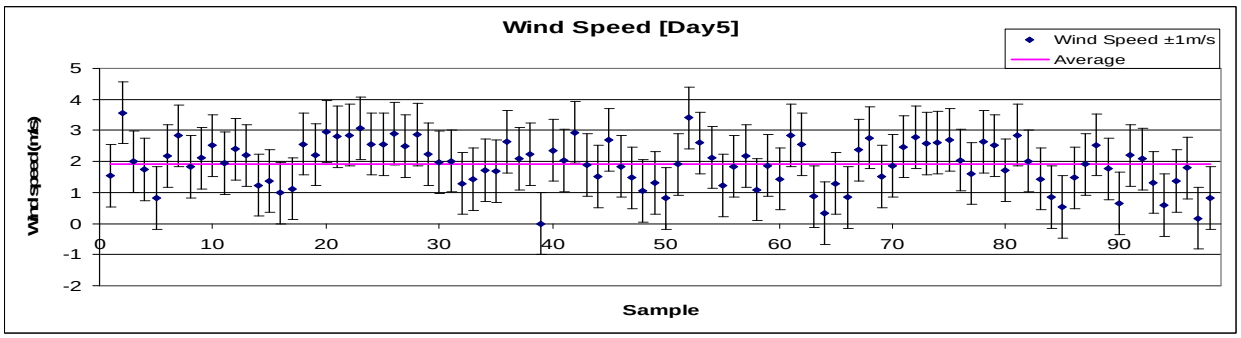
Wind Speed [Day5]
Wind Speed ±1m/s
Average
Windspeed(m/s)
5
4
3
2
1
0
-1
-2
0
10
20
30
40
50
60
70
80
90
Sample